Matter and Radiation at Extremes REVIEW scitation.org/journal/mre

Development of low-coherence high-power laser drivers for inertial confinement fusion

Cite as: Matter Radiat. Extremes 5, 065201 (2020); doi: 10.1063/5.0009319
Submitted: 30 March 2020 • Accepted: 29 June 2020 •
Published Online: 10 November 2020

Yanqi Gao,[1,a)] Yong Cui,[1] Lailin Ji,[1] Daxing Rao,[1] Xiaohui Zhao,[1] Fujian Li,[1] Dong Liu,[1] Wei Feng,[1] Lan Xia,[1] Jiani Liu,[1] Haitao Shi,[1] Pengyuan Du,[1] Jia Liu,[1] Xiaoli Li,[1] Tao Wang,[1] Tianxiong Zhang,[1] Chong Shan,[1] Yilin Hua,[1] Weixin Ma,[1] Xun Sun,[2] Xianfeng Chen,[3] Xiuguang Huang,[1] Jian Zhu,[1] Wenbing Pei,[1] Zhan Sui,[1] and Sizu Fu[1]

AFFILIATIONS

[1]Shanghai Institute of Laser Plasma, China Academy of Engineering Physics, Shanghai 201899, China
[2]State Key Laboratory of Crystal Materials, Shandong University, Jinan 250100, China
[3]School of Physics and Astronomy, Shanghai Jiao Tong University, 800 Dongchuan Road, Shanghai 200240, China

Note: This paper is part of the Special Issue on Progress in Matter and Radiation at Extremes in China.
[a)]**Author to whom correspondence should be addressed:** liufenggyq@siom.ac.cn

ABSTRACT

The use of low-coherence light is expected to be one of the effective ways to suppress or even eliminate the laser–plasma instabilities that arise in attempts to achieve inertial confinement fusion. In this paper, a review of low-coherence high-power laser drivers and related key techniques is first presented. Work at typical low-coherence laser facilities, including Gekko XII, PHEBUS, Pharos III, and Kanal-2 is described. The many key techniques that are used in the research and development of low-coherence laser drivers are described and analyzed, including low-coherence source generation, amplification, harmonic conversion, and beam smoothing of low-coherence light. Then, recent progress achieved by our group in research on a broadband low-coherence laser driver is presented. During the development of our low-coherence high-power laser facility, we have proposed and implemented many key techniques for working with low-coherence light, including source generation, efficient amplification and propagation, harmonic conversion, beam smoothing, and precise beam control. Based on a series of technological breakthroughs, a kilojoule low-coherence laser driver named Kunwu with a coherence time of only 300 fs has been built, and the first round of physical experiments has been completed. This high-power laser facility provides not only a demonstration and verification platform for key techniques and system integration of a low-coherence laser driver, but also a new type of experimental platform for research into, for example, high-energy-density physics and, in particular, laser–plasma interactions.

I. INTRODUCTION

Lasers can concentrate large amounts of energy on very small spatial scales and on extremely short time scales, and are thus among the most effective means to achieve high-energy-density states. Conventional lasers are all characterized by high coherence, narrow linewidth, directionality, and high brightness and have therefore become widely used in fundamental research and in applications in the medical, industrial, military, communications, and other fields. Although traditional high-coherence lasers have provided unprecedented conditions for many areas of scientific research and practical application, the high coherence of the laser can be considered a double-edged sword, since it can lead to unexpected problems arising in certain circumstances. For example, in optical microscopy, environmental scattering causes random phase delays on the particle scale for high-coherence lasers, resulting in interference speckles. This speckle effect will greatly reduce the resolution of the microscope.[1,2] For a fiber-optic gyroscope, the long coherence length is likely to increase the amount of noise caused by Fresnel backreflection, Rayleigh backscatter, the nonlinear Kerr effect, and other factors, thereby reducing the accuracy and sensitivity of the gyroscope.[3] Similar problems arise in laser-driven inertial confinement fusion (ICF).[4] ICF is one of the most promising routes to the generation of clean energy, and there are four leading approaches to its implementation, namely, direct drive, indirect drive, fast ignition, and hybrid drive.[5–8] Whichever driving method is used, laser–plasma instability (LPI) is always a critical problem.[5,9–11] When laser beams propagate through a plasma, processes such as stimulated Brillouin scattering, stimulated Raman scattering, cross-beam energy transfer,

and nonlinear self-focusing occur and have detrimental effects on the fusion process.[12,13] These factors have seriously hindered the achievement of controlled fusion in the laboratory.[14,15] There are two main reasons why high coherence leads to increased LPI:

1. High spatial coherence results in a large number of unstable and unpredictable high-intensity regions distributed in the focal spot. The initial wavefront of the laser beam, which is generally obtained by collimating a near-ideal point light source from a single-mode fiber, is nearly an ideal plane wave. However, during stepwise beam expansion, propagation, amplification, harmonic conversion, focusing, etc., the wavefront quality gradually deteriorates owing to factors such as insufficient surface quality of optical components, thermal distortion, and disturbed air. The reduced wavefront quality leads to spatial interference, which in turn causes multiple strong interference speckles in the focal spot. Consequently there are regions in the spot where the local intensity is excessively high, resulting in increased LPI.
2. High temporal coherence implies a narrow line width and a definite spectral phase relationship. These result in two effects: first, the conditions for the occurrence and growth of parametric instability can be easily satisfied; second, the strong speckle distribution in the focal spot remains stable, and LPI occurs and increases with time.

Since the 1980s, many efforts have been made to overcome these problems. In general, two approaches have been adopted.

The first approach retains the original high-coherence laser drivers and relies on improved beam control (beam smoothing techniques) to reduce the negative impact of coherence. This has been the main direction of laser driver development in recent decades. The smoothing techniques involve two steps. In the first step, two-dimensional near-field phase elements [such as distributed phase plates (DPPs), continuous phase plates (CPPs), and lens array (LAs)] are used to expand the far-field focal spot size of the beam.[16–19] The middle- and low-frequency components of the focal spot intensity distribution are spatially shaped to obtain a uniform profile, reducing the probability of ultrahigh power densities occurring and thereby reducing the degree of LPI. In the second step, the smoothing by spectral dispersion (SSD) technique[20] is used to broaden the spectral width of the original beam through phase modulation. Then, in combination with a grating, a time-varying angular sweep of the beam speckles (corresponding to a spatial sweep of the speckle positions) in the focal area is introduced to perform temporal smoothing. The broadening of the spectrum and the spatial variation of the speckle distribution with time in this step are expected to have a positive effect on the suppression of LPI.[21]

The second approach is to develop a brand new low-coherence laser driver to directly obtain a low-coherence driven source with lower temporal and spatial coherence and better smoothing. In general, there are two ways to obtain a low-coherence driven source. One way uses a pulse source with low temporal and high spatial coherence so that, after propagation, amplification, and harmonic conversion, a high-energy laser pulse with low temporal and high spatial coherence is produced. A beam smoothing technique [e.g., induced spatial incoherence (ISI)[22]] is then applied to give a driving field with low temporal and low spatial coherence. The other way is to use a pulse source with low temporal and low spatial coherence directly. After propagation, amplification, and harmonic conversion, a high-energy driving pulse with low temporal and low spatial coherence is obtained.[23]

The use of traditional high-coherence laser drivers together with beam smoothing techniques has always been the mainstream approach to reducing LPI in ICF. Facilities based on this approach, represented by Nova, OMEGA, the National Ignition Facility (NIF), Laser Mégajoule, GEKKO, and the Shenguang series, have made great contributions to ICF research.[12,24–29] Moreover, a large number of experimental and theoretical studies have shown that the decoherence techniques used in current laser drivers, such as CPPs,[18] SSD,[20] and polarization smoothing (PS),[30] can suppress the detrimental effects of LPI under certain conditions. However, some researchers in the field of ICF believe that low-coherence drivers, which have greater output bandwidth and lower temporal and spatial coherence, may have a better smoothing effect and greater potential to suppress or even completely overcome LPI, and they have therefore suggested that using low-coherence light with broad bandwidth is a viable alternative approach.[5,12,31–33] In the 1990s, many laboratories explored the use of low-coherence light in a series of facilities, including Pharos III, Gekko XII, PHEBUS, and Kanal-2.[23,34–36] However, the progress of these investigations was hampered by the level of development of laser technology at the time, and they encountered many bottlenecks and difficulties related, for example, to the generation of low-coherence sources, the efficient amplification and safe propagation of low-coherence pulses, and the efficient harmonic conversion of low-coherence pulses. In the subsequent decades, it generally came to be accepted that ignition would be realized based on traditional high-coherence lasers combined with beam smoothing techniques (CPP + SSD + polarization smoothing).[37,38] In addition, there was a lack of significant progress both in the key technology of low-coherence drivers and in studies of the interaction between low-coherence light and matter.[39] Thus, research into low-coherence laser driver technology basically stagnated. However, with the activation of the NIF, and especially with the completion of the National Ignition Campaign, it became clear that the suppressive effects of existing decoherence methods based on beam smoothing of high-coherence lasers are limited and that this approach is unable to overcome LPI completely. There is a need for further substantial reductions in the temporal and spatial coherence of driving pulses. In this context, efforts have resumed to explore the feasibility of low-coherence laser drivers.[40–42]

To overcome the technical bottlenecks that have limited the development of low-coherence drivers, such as those related to generation and control of low-coherence sources, broadband amplification, high-efficiency harmonic conversion, and beam smoothing of low-coherence pulses, our team has carried out a series of key studies since 2016.[43–50] The superluminescent diode (SLD) has been introduced into the ICF field for the first time as a lower-coherence seed source. When this is combined with precise temporal shaping and spectral control techniques, the temporal and spectral profiles of a low-coherence pulse can be precisely shaped. In the amplification sections, multilevel spectral shaping filters have been adopted to suppress the spectral narrowing of the laser system. Under high-gain conditions ($>10^7$ times), with Nd:glass rod amplifiers, a low-temporal-coherence pulse with tens of joules of energy and a large bandwidth (15 nm) has been created. The corresponding coherence time is only 270 fs. With Nd:glass disk amplifiers, a kilojoule-level,

several-nanosecond pulse with a bandwidth of 13 nm and a coherence time of 290 fs has been produced without damage. A new approach to harmonic conversion of low-temporal-coherence pulses has allowed low-coherence second-harmonic generation (SHG) with an efficiency of up to 70% and a bandwidth of 3 nm with the use of a potassium dideuterium phosphate (DKDP) crystal. A 520 J pulse with a coherence time of 300 fs has been produced by using a large-aperture potassium dihydrogen phosphate (KDP) crystal. A beam smoothing technique combining a LA or a CPP with the ISI method gives a focal spot with good uniformity and a fast smoothing time. The low-coherence laser facility, named Kunwu, provides a new type of experimental platform for a variety of studies, including those of laser–plasma interaction and high-energy-density physics.

The structure of the remainder of this paper is as follows. Section II gives an overview of the historical development of low-coherence high-power laser drivers. The subsequent sections describe the techniques developed in our institute for generation and control (Sec. III), broadband amplification (Sec. IV), efficient frequency conversion (Sec. V), and temporal and spatial beam smoothing (Sec. VI) of low-coherence pulses. Finally, Sec. VII is devoted to our conclusions.

II. HISTORICAL DEVELOPMENT OF LOW-COHERENCE HIGH-POWER LASER DRIVERS

To aid the development of ICF based on low-coherence laser drivers, the key techniques involved and the ways in which they are integrated have been investigated in many high-power laser laboratories around the world. The most representative of these facilities are Gekko XII, PHEBUS, Pharos III, and Kanal-2. In this section, we will use the results of the work done in these facilities to analyze key aspects of low-coherence drivers, including source generation, amplification, harmonic conversion, and beam smoothing of low-coherence pulses.

A. Low-coherence light source

In a high-power laser facility, the system starts with the front-end laser source. Its main function is to provide different kinds of seed sources for the laser system as a whole and to control various properties of the laser pulse, such as the temporal pulse shape, the spectral characteristics, and the spatial intensity distribution.[51–53] In the last two decades, research on low-coherence front-end sources has been carried out in a number of countries, including Japan, the USA, France, and Russia. In the following subsections, different front-end techniques are analyzed and compared.

1. Partially coherent (both temporal and spatial) light source based on amplified spontaneous emission

In the 1990s, Nakano and co-workers reported the characteristics of a partially coherent light source for the high-power Nd-phosphate glass laser system Gekko XII at the Institute of Laser Engineering, Osaka University.[35,54,55] The amplified spontaneous emission (ASE) front-end system consisted of an ASE generator, a four-pass rod amplifier, a spectral disperser, and a pulse shaper. A flash-pumped Nd:glass rod with a diameter of 25 mm and a gain length of 300 mm (Hoya LHG-8, 2 wt. % Nd_2O_3) was used to produce ASE light. The structure of the ASE generator was similar to a concave–convex cavity, which gives increased temporal and spatial coherence. After the four-pass rod amplifier, the pulses were amplified to 10 μJ/ns with a nominal gain of 10^7. As a result of the finite spectral response of the four-pass rod amplifier, the spectral width was narrowed to less than 2 nm. A pulse selector consisting of three Pockels cells with 12 polarizers was used to shape the pulse width. Owing to the rise time of the driver, the shortest pulse duration obtained was limited to 1 ns. Anyway, owing to the constraint imposed by the spatial and temporal modes, this type of source based on ASE still has relatively high temporal and spatial coherence and thus is not the ideal low-coherence light.

2. Low-spatial-coherence laser source based on a mode-locked oscillator

Another method for generating partially coherent light on Gekko XII used a mode-locked oscillator and multimode optical fibers.[56] Instead of the ASE broadband oscillator described above, the oscillator here was an actively mode-locked Nd-doped yttrium lithium fluoride (Nd:YLF) oscillator, which generated a train of transform-limited 120-ps pulses at a central wavelength of 1053 nm. Obviously, this was a high-temporal-coherence laser oscillator. The spectral width was adjusted to about 0.6 nm. A grating pair then compressed the chirped pulse to 15 ps, which is approximately equal to the coherence time. A pulse sequence with a separation of 100 ps was produced through a 32-channel fiber divider and coupler. The output pulse train was incident into a step-index multimode fiber to reduce the spatial coherence. The core size, length, and numerical aperture of the multimode fiber were 200 μm, 200 m, and 0.2, respectively. The beam divergence of the mode dispersed beam was about 66 times diffraction-limited. In other words, the light source had very high temporal coherence and relatively high spatial coherence, even with the use of a multimode fiber to induce spatial incoherence.

3. Q-switched low-coherence laser sources

a. Q-switched source based on Nd:glass. In work at the Kanal-2 facility at the N. G. Basov Quantum Radiophysics Division of the P. N. Lebedev Physical Institute in Russia, both the number of transverse modes and the spectral width were varied.[39,57] A master oscillator provided the required spatial and temporal coherence of a radiation pulse for ICF experiments. The master oscillator of the Kanal-2 laser facility (see Fig. 1 in Ref. 39) is based on a confocal cavity with a base length of 1200 mm. A Nd:glass rod with a length of 300 mm and a diameter of 10 mm is used as the gain medium. An electro-optical Kerr shutter that allows operation with a wide range of divergence angles of the generated radiation is used as a Q-switch. Obviously, this is an actively Q-switched cavity, which has high temporal coherence. In the cavity center, a forming diaphragm is used to control the number of transverse radiation modes, and a collective lens with a focal length of 300 mm is used to provide a uniform distribution of transverse mode radiation over the image area in the diaphragm, so that the image formed in the diaphragm plane is optically transmitted to the target. By altering the diameter of the diaphragm, the divergence and spatial coherence of the radiation from the generator can be varied in the range of 1.33×10^{-2} –3×10^{-3} rad. The spatial and angular distributions of the output radiation can be controlled by changing the shape and transmission profile of the

diaphragm. The pulse duration and contrast are controlled by two series-synchronized Kerr gates. The number of transverse modes for both linearly polarized and partially polarized radiation can be in the range N = 100–1000. The pulse duration is 2.5 ns and the output bandwidth is 2.6 nm. It is quite clear that, to some extent, the master oscillator of the Kanal-2 laser facility is a high-temporal-coherence and relatively high-spatial-coherence laser source.

b. Q-switched source based on mixed glasses. The output pulse capabilities of the PHEBUS laser facility at the Limeil-Valenton laboratory in France were reported in the 1990s.[58,59] The layout of the large-spectral-bandwidth oscillator based on mixed glasses can be found in Fig. 11 in Ref. 58. A silicate glass rod and a phosphate glass rod were coupled into the same cavity to obtain a large spectral bandwidth. The bandwidth could be adjusted between 1 nm and 2.5 nm by varying the pumping levels of these two rods. This type of broadband source was an actively Q-switched cavity oscillator, and, as a result, the output still had high temporal and spatial coherence. The output beam was injected into a multimode fiber of core diameter 100 μm and length 50 m to reduce the spatial coherence of the source. The output from such a multimode fiber should be regarded as an extended source rather than a point source. Therefore, spatial filters were applied to relay the image of the fiber output through the whole laser amplifying section. The fiber was able to propagate about 1000 modes, and thus the large number of overlapping speckle patterns led to spatial smoothing. The energy of the fiber output was about 1 μJ. The temporal pulse shaping was obtained through a Pockels cell. By varying the electrical voltage applied to the electro-optic crystal, a variety of laser pulses could be obtained (see Fig. 4 in Ref. 58). Although this was a broadband source, it still had a relatively high temporal coherence due to the Q-switched cavity. Therefore, the spatial coherence was also not very low.

c. Q-switched source with etalon for spectral expansion. The U.S. Naval Research Laboratory (NRL) also carried out some studies with broadband Nd:glass laser radiation using the Pharos III laser system.[34] The oscillator produced a 40-ns pulse in the TEM_{00} mode. It is clear from the structure of the oscillator (see Fig. 9 in Ref. 34) that this was an actively Q-switched cavity. Therefore, the pulses had relatively high temporal and spatial coherence. The spectral width could be altered by an angle-tuned etalon. The laser spectrum of variable bandwidth (15 cm^{-1}–22 cm^{-1}) was acquired by using diverse combinations of etalons and controlling the round-trip cavity gain. The oscillator pulse was sliced to a 2.5-ns Gaussian-like pulse by two Pockels cells with about 1-ns risetime, and the contrast ratio was greater than 10^6. Although the Nd:glass oscillator was a broadband source, it still had relatively high temporal and spatial coherence, and the spectral phase was highly correlated.

As described above, some laboratories have adopted a variety of techniques in attempts to obtain ideal low-coherence light, but all these seed sources have similar cavity structures or Q-switched and even mode-locked cavities. The output pulses usually have relatively high temporal coherence despite the barely satisfactory bandwidth. The main characteristics of the different sources are compared in Table I. All these partially coherent sources have relatively high temporal and spatial coherence. In addition, it is difficult to obtain highly dynamic and precise shaping of pulses using Pockels cells. However, precise temporal shaping is a prerequisite for achieving low-entropy compression, reducing the energy requirements on the target and decreasing the scale and cost of the laser facility.[60]

B. Amplification

Whether the laser source is ASE or some other broadband oscillator, it needs to be amplified to achieve the high energies required for applications. In the low-coherence large-scale laser facilities discussed here, the typical amplification process was to inject the low-coherence front-end source with temporal and spatial shaping into a Nd:glass amplification chain. High-energy output pulses were obtained by means of the gain of the Nd:glass system.

1. Amplification of partially coherent (both temporal and spatial) sources based on ASE

The amplification and propagation of partially coherent ASE from a high-power Nd:glass system was first demonstrated on the Gekko XII laser facility. The amplification chains of Gekko XII are divided into a preamplifier and a main amplifier.[28] The preamplifier consists of four rod amplifiers each with a diameter of 25 mm. The main amplifier includes two 50-mm-diameter rod amplifiers and five disk amplifiers, and the beam size at its output is 320 mm.

After the injected ASE (about 0.5 μJ, 1.6 nm, 3 ns) was amplified by the amplification chain, the energy reached 800 J and the spectral width was typically 1.3 nm (the corresponding flux of the main amplifier output was 1 J/cm^2 and the power density was 0.3 GW/cm^2).[54] No remarkable gain reduction or spectral narrowing were found during the amplification process with the incident spectral width in the range of 0.1 nm–2.0 nm. To better understand the gain characteristics and spectral changes of the ASE pulse, numerical simulations were performed based on an extension of the Frantz–Nodvik equation.[61]

TABLE I. Main characteristics of different sources.

Source type	Facility	Country	Coherence		Temporal shaping capability
			Temporal	Spatial	
ASE	Gekko XII	Japan	Relatively high	Relatively high	Low
Mode-locked oscillator	Gekko XII	Japan	Very high	High	Low
Q-switched laser source	Kanal-2	Russia	High	Relatively high	Low
	PHEBUS	France	High	Relatively high	Low
	Pharos III	USA	High	Very high	Low

The results were in good agreement with the experimental measurements.

It is well known that amplification and propagation of high-coherence light always induces hot-spot structures in the far-field region owing to the phase-front distortion in the near-field. However, this is not the case for partially coherent light, because the nonuniform irradiation distribution causes an interference effect that undergoes rapid temporal changes owing to the short coherence time compared with the pulse duration. Compared with traditional lasers, the uniform output radiation in the quasi-far-field region is predictable for ASE. It is worth noting that the temporal profile of the amplified ASE has complex fine intensity spikes with a duration of about the reciprocal of the frequency width, and the spatial profile as measured by a streak camera is random, as shown in Fig. 3 in Ref. 54. The instantaneous speckles of the ASE may cause nonlinear index effects in the glass, risking damage to the amplifying element and severely limiting the output capability of the system. The main reason for this is that the partially coherent source employed (an ASE source generated by the method described in Sec. II A 1) has relatively high temporal and spatial coherence.

2. Amplification of low-spatial-coherence laser source based on a mode-locked oscillator

When pulses from the actively mode-locked Nd:YLF oscillator described in Sec. II A 2 were injected into the Gekko XII amplification system, an output beam of energy 120 J and diameter of 320 mm was obtained.[56] Few reports of results with this setup are available. However, according to our understanding, both the temporal and spatial coherence of these pulses are the highest among all of the sources mentioned above, so the temporal and spatial characteristics of the pulses after amplification and propagation should be the poorest. The corresponding safe output capability of the facility would thus be the lowest, and therefore a facility with this source will be of no practical value. A comparison of the output energies reported above confirms this.

3. Amplification of Q-switched low-coherence laser sources

a. Amplification of a Q-switched source based on Nd:glass. The Kanal-2 laser facility consists of a master oscillator, preamplifier, and serial cascade amplifiers.[39] The most characteristic feature of this facility is that the degree of radiation coherence is controllable, both spatially and temporally. Adjustable parameters of the laser radiation include the angle of divergence, the number of transverse modes, and the width of the laser line. The spatial and temporal characteristics of the laser are controlled by the Q-switching master oscillator.

The amplifier system consists of several cascaded 680-mm Nd:glass rods made of GLS-1 silicate glass and of various diameters (from 20 mm to 60 mm). The output aperture diameter of the beam in the linear cascade amplifier is 60 mm. The pulse duration is 2.5 ns and the maximum radiation energy is 300 J. The divergence of the amplified pulse is 1.1×10^{-3}. The output spectral bandwidth is 2.6 nm, with a central wavelength of ~1060 nm. Because of strong heating of the active elements of the amplifier, there is partial depolarization of the linearly polarized radiation by 5% or more. owing to its low coherence, the multimode radiation from this facility has many potential advantages compared with conventional high-coherence lasers, including high homogeneity without speckling of target irradiation, suppression of small-scale self-focusing, a simple optical scheme, a reduced total number of optical elements in the amplifier, simpler requirements for these elements, and no need for spatial filters, vacuum channels, or a wave-front corrector. In addition, the relatively broad bandwidth may improve the amplification gain in the saturation regime if the lasing linewidth is increased to a value comparable to the luminescence linewidth of the active medium. These advantages, however, need to be verified by further experiments.

b. Amplification of a Q-switched source based on mixed glasses. The high-power PHEBUS Nd-glass laser facility delivered a 2×10 kJ pulse with a duration of 1.3 ns when a narrowband coherent laser was used.[58] The laser amplifier, consisting of three sections, namely, a preamplifier, a driver, and a power section, provided an overall gain of 10^8. The beam was amplified to the joule level and spatially shaped in the preamplifier section. The drive amplifier section consisted of seven rod amplifiers with four different diameters. The power section was composed of five 31.5-cm and four 46-cm amplifiers and amplified the energy to 300 J–10 000 J.

The front end of the PHEBUS laser facility was a phosphate-glass broadband oscillator with a bandwidth of 1 nm. The point source could be converted into an extended source by means of a multimode fiber, thereby reducing the spatial coherence of the beam. Compared with the standard configuration, the output power in this configuration was limited by a saturation-like effect, and the top of the laser pulse was "scraped" by the strong reduction in temporal fluctuations in the amplification stage (see Fig. 11 in Ref. 23).[23,62]

To further understand the physical processes occurring during amplification of partially incoherent light, a series of decomposed amplification experiments were conducted to evaluate the influence of spatial incoherence (geometrical source extension) and temporal incoherence (a broadband spectrum). To investigate the influence of spatial coherence, the output of a narrowband oscillator was injected into the fiber. The power peaked at about 7 TW in the standard configuration. However, a power limit of 3.3 TW was observed in the case of the beam that had been spatially smoothed by the multimode fiber. The influence of low temporal coherence was investigated by injecting the output of a broadband oscillator into the standard configuration. The power limit in this case was 5.2 TW, larger than that with the extended source, revealing that the power limitation mainly resulted from spatial incoherence (an extended source) rather than temporal incoherence (a wider spectral bandwidth).

In addition, strong spectral broadening was observed during the process of amplification: the output spectral width increased to 2.4 nm in the unsaturated regime and 3.4 nm in the saturated regime (see Fig. 8 in Ref. 62).

To completely understand the pulse scraping and power limitation effects in the amplification of partially coherent pulses in a high-power laser chain, a nonlinear statistical model was established to explain the anomalous intensity saturation effect. Experimental and theoretical data revealed the origin of the power limitation encountered on PHEBUS[63–66] to be a combination of nonlinear effects, including self-phase modulation, self-focusing, two-photon absorption, and Kerr electronic nonlinearity. At the root of these processes is the fact that the temporal coherence and spatial coherence

are too high with a Q-switched source, leading to deterioration of time-domain and spatial-domain modulation.

c. Amplification of a Q-switched source with etalon for spectral expansion. The amplifier chain of the Pharos III laser system at the NRL was based on Nd-doped phosphate glass.[34] It consisted of a double-pass rod amplifier of diameter 45 mm and three disk amplifiers with clear apertures of 66 mm, 105 mm, and 150 mm, respectively. The input pulse from the oscillator of an actively Q-switched cavity was light with relatively high temporal and spatial coherence. The spectral line shapes of TEM_{00} mode pulses with pulse duration 2.5 ns could be tuned by an etalon in the oscillator. To ameliorate the high-intensity spatial fluctuations caused by nonlinear phase shifts, intensity-dependent depolarization, and breakup during the process of amplification in the system, image-relaying telescopes and a spatial filter were adopted. Nevertheless, Pharos III was not tightly spatially filtered. The beam expanded from 45 mm to 150 mm in diameter, and the near field of the beam had a flat-topped intensity profile with local nonuniformities of less than ±50% on average. The output energy of the laser was 800 J/beam, with a central wavelength of 1054 nm. The spectral bandwidth at the output of the broadband Nd:glass system could be controlled from 15 cm^{-1} to 30 cm^{-1} by changing the parameters of the oscillator. The coherence time was typically ~1 ps. Measurements of depolarization revealed that the amplified light was linearly polarized to better than a few percent. The far-field quality was about seven times diffraction-limited. Thus, the beam quality was adequate for second-harmonic conversion experiments.

Judging from the amplified output characteristics of the different types of temporally and spatially partially coherent sources described above, the lower the temporal coherence, the weaker are the adverse effects of modulation in the time and spatial domains, and the higher and closer to the limit is the output capability of the corresponding facility. The higher the coherence (under the conditions of not completely coherent light), the more obvious is the degradation of temporal and spatial characteristics, and the lower is the output capability of the facility.

C. Frequency conversion

Second-harmonic generation (SHG) was first demonstrated by Franken *et al.*[67] at the University of Michigan, Ann Arbor, in 1961. This demonstration was only possible because of the invention of the laser, which produced the required high-intensity coherent light. A theoretical foundation for SHG was initially presented in 1962 by Bloembergen and Pershan,[68] who obtained solutions of Maxwell's equations at the planar interface between a linear and a nonlinear medium, taking account of the conditions of energy and momentum conservation.

Taking type I phase matching in a KDP crystal as an example, an extraordinary frequency-doubled photon is generated by two ordinary light photons, both of which are fundamental waves. The phase-matching condition can be written as

$$\hbar\mathbf{k}_{\omega}(\omega) + \hbar\mathbf{k}_{\omega}(\omega) = \hbar\mathbf{k}_{2\omega}(\omega, \theta). \tag{1}$$

In Ref. 68, two parameters are introduced to describe the requirements for efficient SHG:

$$\eta = C^2 I l^2, \quad \delta = \Delta k \frac{l}{2}, \tag{2}$$

where C is a quality parameter characterizing the nonlinear effect of the crystal, I is the intensity of the fundamental frequency, l is the crystal length, and $\Delta k(\omega, \theta) = 4\pi[n(2\omega, \theta) - n(\omega)]/\lambda$. In general, η is about 4–5, $\delta \ll \pi/10$, and Δk is a function of frequency and angle in the crystal at room temperature, which can be expanded in a Taylor series at the phase-matching angle:

$$\Delta k = \Delta k(\omega_0, \theta_0) + \frac{\partial \Delta k(\omega_0, \theta_0)}{\partial \theta}(\theta - \theta_0) + \frac{\partial \Delta k(\omega_0, \theta_0)}{\partial \omega}(\omega - \omega_0) + \cdots. \tag{3}$$

In general, any wave-front distortion or spectral broadening will decrease the efficiency of frequency doubling. Efficient harmonic conversion of low-coherence pulses is a major technical obstacle that hinders the development of low-coherence high-power laser facilities.

Previous research on the harmonic conversion of low-temporal-coherence pulses has mainly focused on the problem of how to achieve group-velocity matching under large-bandwidth conditions. For broadband lasers, the overall group-velocity mismatch between the fundamental wave and the second-harmonic wave in the crystal needs to be sufficiently small compared with the fundamental pulse coherence time.[34,69] Several methods have been implemented to compensate for group-velocity mismatching, and these can be divided into two categories. The first category of methods are based on the use of special geometries and include achromatic phase matching,[34,69,70] multicrystal sequences,[71] tilted quasi-phase-matched gratings,[72] and Čerenkov phase matching.[73] These methods are difficult to implement given the restrictions imposed by the need for beam alignment, and the efficiency of frequency doubling when they are used is lower than that predicted theoretically. The second category use so-called spectrally noncritical phase matching,[74–79] which takes advantage of the fact that there exists a zero-group-velocity mismatching wavelength of SHG for a specific crystal, the conditions for which can be written as

$$\Delta k(\omega_0, \theta_0) = 0 \quad \text{and} \quad \frac{\partial \Delta k(\omega_0, \theta_0)}{\partial \omega} = 0. \tag{4}$$

In this case, the doubling configuration is just like the conventional one, and no modification of the input light is needed, which makes this approach more practical in terms of simplicity, reliability, and conversion efficiency. Fortunately, partially deuterated KDP was found to be suitable for broadband SHG in the region from 1.034 μm to 1.179 μm.[79] This is very important for the Nd:glass lasers that are used to study ICF. Some of the approaches mentioned above have been adopted in Nd:glass facilities. Schemes such as time walk-off compensation, angular dispersion compensation, and chirp modulation matching are reviewed below.

1. Group-velocity mismatch compensation with multicrystals

Pronko *et al.*[34] used two type II KDP crystals in a quadrature arrangement for frequency doubling of broadband high-peak-power Nd:glass laser radiation. The quadrature configuration compensates

for group-velocity mismatching because the transverse projections of the principal axes of the two crystals are orthogonal, as shown in Fig. 1. Hence, the fundamental component, which is polarized along the slow axis in the first crystal, will be polarized along the fast axis in the second. If the thickness of the second crystal is twice that of the first, the walk-off will be compensated, and the second harmonic will be generated efficiently along most of its path. This method has been verified on the Pharos III laser. The bandwidth of the fundamental wave is about 2 nm, which is composed of multilongitudinal modes. The conversion efficiency can reach 55% at a pumped intensity of ~1 GW/cm^2. The main disadvantage of this method is that the output second-harmonic pulses have random polarization. Also, the conversion efficiency will decrease with larger bandwidth. In Ref. 80, it was reported that the first and second crystal were detuned in opposite directions to correspond to different matching wavelengths, and the acceptance bandwidth could be up to 10 nm with optimization. Experimentally, the conversion is found to be nearly 60% for a chirped pulse of bandwidth about 3.2 nm. However, the frequency-doubled light suffers temporal distortion during the depolarization.

Eimerl *et al.*[81] proposed a broadband frequency-tripling method using a crystal cascade as shown in Fig. 2. This method has been demonstrated experimentally for radiation of 1 nm bandwidth on the OMEGA facility[82] at the University of Rochester.[83] The principle is similar to quasi-phase matching: when the phase difference $L\Delta k$ of the three waves in the crystal reaches a value of π, "back-conversion" will occur, that is, the light generated will return to the fundamental wave and the second harmonic. Dispersion by the air in the gap between the two crystals can be utilized to suppress this back-conversion. Theoretically, the conversion efficiency can exceed 70% for 300-GHz bandwidth (1053 nm), but the three-wave phase difference is related not only to the detuning angle, but also to the pump intensity.

2. Group-velocity mismatch compensation with grating angular dispersion

Spontaneous radiation or chirped pulses were used as the seed in the Gekko XII facility, with a bandwidth of about 1 nm.[35] The angular dispersion $d\theta/d\lambda$ of spectral dispersion smoothing was about 239 μrad/nm, which is equal to the wavelength-dependent phase-matching angle near 1053 nm in KDP for type II frequency doubling. This was used to compensate for the phase mismatching caused by the broader bandwidth, and the frequency-doubling conversion efficiency was about 50% with a pumping intensity of ~0.3 GW/cm^2. In fact, group-velocity mismatching is not obvious at 1053 nm for type I SHG, as long as the pump light intensity is increased. The crystal thickness can be appropriately reduced to obtain high efficiency for 1 nm–2 nm bandwidth.

A similar design was applied in the PHEBUS facility.[59] The seed from the multimode oscillator was amplified by the Nd:glass system, and a spatial chirp was then introduced through a grating pair, such that different positions on the beam cross section corresponded to different frequencies.[59] A cylindrical lens placed downstream provided angular dispersion. If the change of the crystal matching angle with frequency was consistent with this angular dispersion, a relatively efficient broadband frequency doubling could be achieved. It was reported that the frequency-doubling conversion efficiency was ~30% for a beam with a bandwidth of 3 nm. This low conversion efficiency could have been caused by the complicated beam alignment and poor beam quality.

3. Group-velocity mismatch compensation with phase modulation

Migus[84,85] and Qian[86] both proposed a broadband frequency-doubling and -tripling method based on pulse chirp modulation. As illustrated in Fig. 3 (see Ref. 84), the phase mismatch is a function of time for a chirp pulse. If the chirp parameter is chosen to make $\Delta k = 0$,

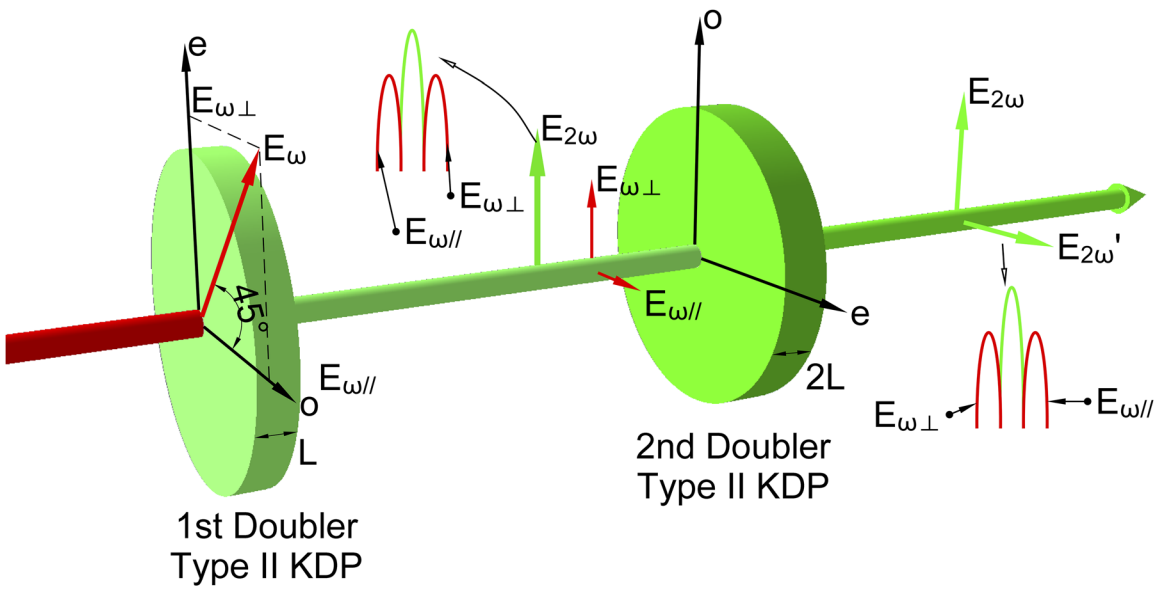

FIG. 1. SHG with two type II crystals in quadrature.

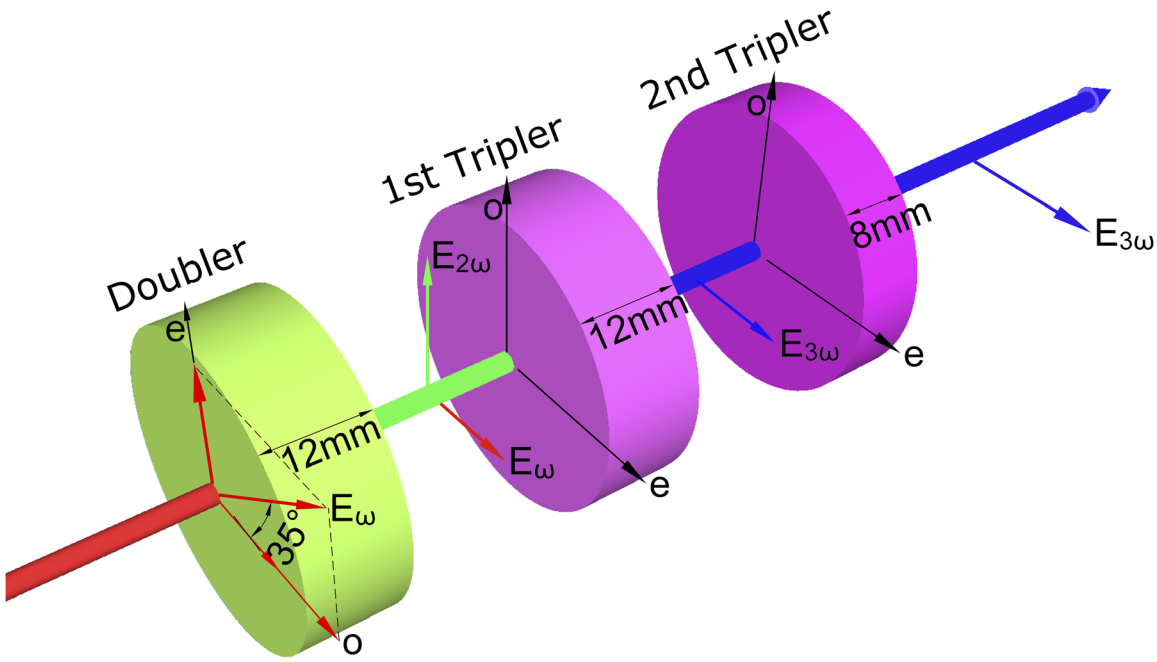

FIG. 2. Broadband frequency tripling with two triplers for the OMEGA facility.

then the conversion efficiency can be significantly increased. This approach was demonstrated experimentally by Raoult *et al.*[84] The bandwidth of the triple frequency was about 1.2 nm, and the pulse could be compressed to 220 fs. However, this method has not yet been applied at any high-power laser facility, possibly because of its complexity.

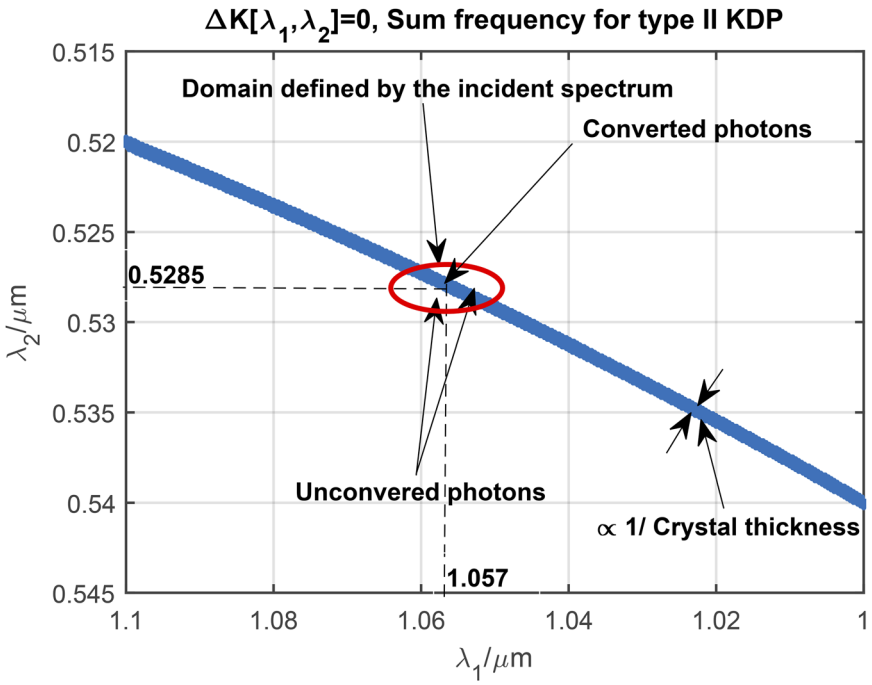

FIG. 3. Phase-matching curve for frequency tripling of chirp pulses. Reprinted with permission from Raoult *et al.*, Opt. Lett. **24**(5), 354-356 (1999). Copyright 1999 Optical Society of America.

Chen *et al.*[87] demonstrated that the tripling scheme can support a bandwidth as large as 5 nm if the effects of group-velocity mismatching are ameliorated through frequency mixing of a broadband chirped pulse with a narrowband laser pulse.

4. Wavelength-insensitive phase-matched SHG in partially deuterated KDP

The aforementioned schemes are too complicated to implement in large laser facilities. Adopting a different approach, Webb *et al.*[79] experimentally determined the spectrally noncritical phase-matching behavior of type I SHG in KDP and its dependence on the deuteration level in partially deuterated KD*P. The first-order wavelength–sensitivity parameter $\partial k/\partial\omega$ for type I SHG of 1.053 μm light vanishes for a KD*P crystal with a deuteration level of 12% ± 2%. Using this configuration, Zhu *et al.*[88] experimentally and numerically investigated the characteristics of SHG with a femtosecond laser at 1 μm. They found that it was possible to support efficient SHG over 20 nm bandwidth of the fundamental wave at 1 μm in a 10-mm-long crystal. As suggested in Ref. 79, this method can be utilized for large-aperture beams, and KDP analogs are the only suitable crystals.

Many other concepts have been proposed for broadband frequency doubling or tripling. By applying a longitudinal gradient temperature field to a lithium triborate (LBO) crystal, Rozenberg and Arie[89] were able to achieve an acceptance bandwidth of SHG reaching ~10 nm. Yuan *et al.*[90] proposed that the acceptance bandwidth of frequency tripling could be improved by using a segmented partially deuterated KDP crystal with discrete values of deuteration.

As is well known, the intensity fluctuation period of a low-temporal-coherence pulse is close to the coherence time. When the pulse duration is far greater than the coherence time, fluctuations of the phase difference between the fundamental wave and the second harmonic caused by the walk-off effect impose the main restriction on the efficiency of SHG. All of the methods described above can reduce these fluctuations and effectively improve the conversion efficiency. However, the methods in the second category are better suited to engineering applications.

As well as group-velocity mismatching, the physical processes involved in harmonic conversion of low-temporal-coherence pulses need to be better understood. The progress that we have achieved so far in this area will be described in subsequent sections. As far as achieving harmonic conversion of low-spatial-coherence pulses is concerned, this mainly requires matching of spatial wave vectors. Low-spatial-coherence pulses are not essential for low-coherence drivers: for instance, in the amplification and harmonic conversion sections, we can use beams with high spatial but low temporal coherence and then induce spatial incoherence during the focusing stage to reduce the spatial coherence of the focused beam. Therefore, we shall not discuss these further in this paper.

D. Beam smoothing in low-coherence high-power laser drivers

In a low-coherence high-power laser system, focal spot conditioning is a key factor affecting energy transfer from the laser to the target. In ICF experiments and equation-of-states determinations, the focal spot needs to be uniform to avoid hydrodynamic instability and LPI. In these experiments, the root mean square (rms) of the focal spot intensity distribution should be a few percent or even less,[91] and this should be achieved within a few hundred picoseconds or even shorter. However, owing to thermal distortion of the amplifying medium, nonideal optics, air disturbances, and so on, the wave front of the output pulse in a real high-power laser system is severely and randomly distorted, and its focal spot distribution is uneven and unstable. To achieve focal spot conditioning in a low-coherence laser system, many beam smoothing methods have been proposed. These methods can be divided into three categories: spatial smoothing methods that can tailor the overall shape of the focal spot, temporal smoothing methods that eliminate speckling by rapidly changing the focal spot details over time, and far-field image transfer methods that have both temporal and spatial smoothing effects.

1. Spatial smoothing methods

Most spatial smoothing methods rely on modulation of the wave front distribution in the near field, as shown in Fig. 4. According to Fresnel diffraction theory, the near field and far field of the light are Fourier transforms of each other. Therefore, the far-field distribution can be modified by modulating the phase of the near field. For low-spatial-coherence light, Fresnel's diffraction law should be used with ensemble theory or statistical optics to predict the effect of phase modulation. The methods using continuous phase plates (CPPs) and lens arrays (LAs) belong to this type.

Random phase plates (RPPs) were proposed in 1984 by Kato *et al.*[17,92] An RPP consists of small blocks of different thicknesses. The phase differences introduced by these small blocks are randomly distributed between 0 and π. The focal spot formed by an RPP is similar to a Gaussian function with speckles. However, sometimes it is more desirable to obtain a flat focal spot with a super-Gaussian distribution, which is one of the disadvantages of RPPs. At the same time, discontinuities in an RPP will cause energy loss due to diffraction. Distributed phase plates (DPPs) were proposed to avoid the energy loss in RPPs, but it is still difficult to design the intensity distribution of the focal spot.[93] Kinoform phase plates were designed for better control of focal spot distribution, but they still suffer from the problem of energy loss.[94] To overcome these shortcomings, CPPs were proposed.[16] Since discontinuities in the phase plate distribution are then avoided, the diffraction efficiency of a CPP can theoretically reach 100%. With appropriate use of a frequency filter and phase unwrapping methods together with the conventional Gerchberg–Saxton method, a CPP can be designed to obtain a far-field distribution with a certain envelope.[95]

The use of LAs was proposed in 1986 by Deng *et al.*[19] In this method, in addition to the main lens, an additional array of lenses is added to obtain quasi-near-field illumination. Ideally, the focal spot of this LA will be the quasi-near field of a single small beam multiplied by the Dirichlet kernel. The diffraction effect of small beams will cause low-spatial-frequency intensity fluctuations, and the Dirichlet kernel will cause high-frequency intensity modulation in the focal spot.

The use of CPPs and LAs is not sensitive to wave-front distortion, because the wave-front modulation introduced by these methods has a higher spatial frequency than the distortion. Therefore, these schemes can be applied to high-power lasers to obtain a relatively stable and flat focal spot. Although those spatial smoothing methods are effective for tailoring the envelope of the focal spot, speckles still exist in the spot. These speckles come from interference of the near field. The size of the speckles is close to the diffraction limit

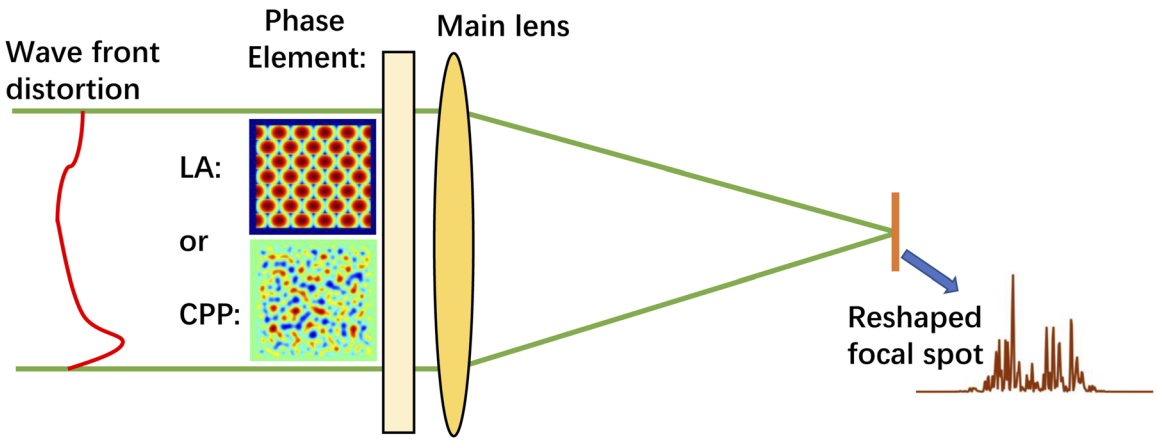

FIG. 4. Focal spot reshaping using a phase element.

of the beam. Temporal smoothing methods need to be used for the suppression of speckles.

2. Temporal smoothing methods

The way to eliminate speckling is to use a temporal smoothing scheme that can smooth the speckles in the far field after a sufficient smoothing time by changing the far field rapidly with time. Temporal smoothing methods for low-coherence lasers mainly include induced spatial incoherence (ISI), angular dispersion of the spectrum, and polarization smoothing. The key factor in temporal smoothing is decorrelation of the near field or the introduction of low spatial incoherence.

ISI was proposed in 1983 by Lehmberg and Obenschain.[22,96] Time delays greater than the coherence time of light are added to different areas of the laser in the near field. In the early ISI experimental design,[97] the delay effect was introduced by using a pair of relatively thick stepped mirrors. On a laser with sufficient bandwidth, a stair-shaped plate can be used to achieve such an effect, as shown in Fig. 5. The whole beam will be divided into small beamlets with different time delays, and these beamlets are incoherent with each other. The incoherent beamlets will be superimposed on the focal plane to eliminate speckles caused by interference. The instantaneous intensity distribution of the focal spot is still speckled and highly uneven. However, this distribution changes rapidly with time, and, after sufficient integration time, a smoothed focal spot intensity distribution without speckles can be obtained.

Angular dispersion of the spectrum was proposed in 1993 by Nakano *et al.*[55] This method is very similar to the smoothing by spectral dispersion (SSD) method,[20,98–101] but the latter is generally used on narrow-bandwidth laser systems.[102] When used in a broadband low-coherence laser system, the SSD method cannot take advantage of the broadband characteristics of the laser. In angular dispersion of the spectrum, different spectral components of the light are dispersed in different directions. On the focal plane, light fields with different frequencies have different displacements owing to

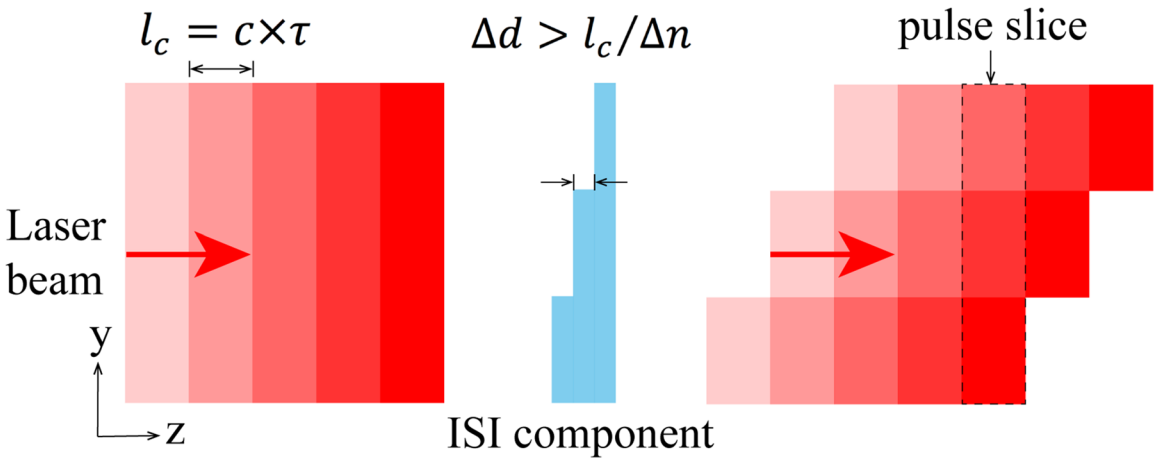

FIG. 5. Schematic of the ISI method. Reprinted with permission from Zhao *et al.*, Appl. Opt. **58**(8), 2121–2126 (2019). Copyright 2019 Optical Society of America.

dispersion, and the total focal spot uniformity is improved because of the intensity superposition. In one-dimensional angular dispersion of the spectrum, the speckles in the direction of dispersion are smoothed, while those in the vertical direction are not completely removed. Two-dimensional dispersion smooths speckles in all directions.

Polarization smoothing is another temporal smoothing method. Its original form was the polarization control plate, which was proposed by Gunderman *et al.*[103] and Tsubakimoto *et al.*[104] However, a simpler device can be used for polarization smoothing. If birefringent material is used,[30,105] the beam is divided into two perpendicular polarized beams with slightly different angles, and their focal spots are added by intensity to obtain an instantaneous smoothing effect. Although it is mainly used on conventional narrow-bandwidth laser systems, polarization smoothing can also be applied to low-coherence laser systems.

When the above methods are adopted, temporal smoothing is realized by artificially reducing the spatial coherence of the beam. There is some freedom in the placement of these additional optical components in the optical chain. For example, we can place the ISI plate in front of the final focusing lens or with the spatial filter in front of the main amplifier. However, in the second case, the effect of low spatial coherence on the propagation, amplification, and frequency conversion of the beam needs to be estimated.

3. Far-field transfer method

Smoothing methods based on far-field image transfer are mainly used on low-spatial-coherence sources, where they have both temporal and spatial smoothing effects. Echelon-free ISI[22,106] on the Nike laser and partially coherent light smoothing on PHEBUS belong to this type of beam smoothing method. In these methods, the far-field shape (i.e., the divergence angle) of the beam is directly adjusted by the mode-limiting hole (or the end face of the multimode fiber) before the amplification stage. After amplification, the far field of the beam reaches the target through image transfer. In this way, the number of spatial modes determines the smoothed spatial distribution. Speckles can be eliminated by using large numbers of spatial modes. In these methods, image transfer is able to control the focal spot shape because low-spatial-coherence light has large divergence angles, and so distortion in the optical path has little effect on the far-field shape.

The echelon-free ISI method is an improved version of traditional ISI and can be employed on low-spatial-coherence lasers, such as KrF lasers. Figure 6(a) shows the echelon-free ISI on the Nike KrF laser. By using a broadband ASE oscillator source, and based on the principle of image transfer, the shape of the focal spot can be changed directly by controlling the variable-density absorber at the front. In the PHEBUS facility based on a Nd:glass laser, the beam smoothing method used is called partially coherent light smoothing.[107] This method utilizes the spatial mode dispersion of a multimode fiber to obtain low-spatial-coherence light, as demonstrated in Fig. 6(b). With proper design of the image transfer system of the beam, the focal spot is expected to be an image of the multimode fiber output surface. Both methods utilize image transfer of a low-spatial-coherence laser to obtain the desired focal spot shape. Instantaneously, the focal spot still has a distribution of speckles. However, with image transfer, the

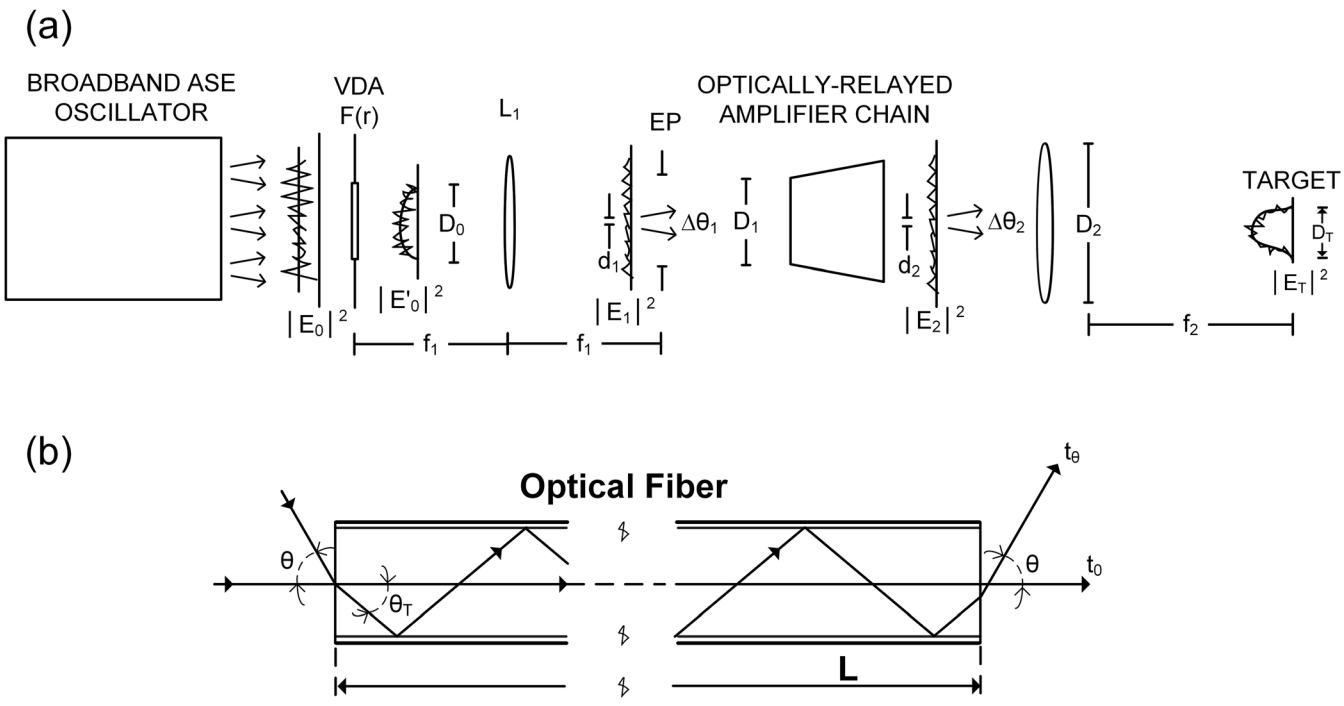

FIG. 6. (a) Demonstration of the echelon-free ISI method. Reprinted with permission from Lehmberg *et al.*, J. Appl. Phys. **62**(7), 2680–2701 (1987). Copyright 1987 AIP Publishing LLC. (b) Spatial mode dispersion in the optical fiber smoothing method. Reprinted with permission from Veron *et al.*, Opt. Commun. **65**, 42–46 (1988). Copyright 1988 Elsevier.

statistical characteristics of the low-spatial-coherence light ensure that the focal spot distribution tends to become flat after sufficient smoothing time. Far-field transfer methods can obtain a focal spot with excellent uniformity (i.e., rms < 1%), as reported for the Nike facility.[105] The disadvantage is that the propagation of a low-spatial-coherence laser with large emission angle increases the complexity of the laser system.

As mentioned above, many efforts have been made to obtain low-coherence high-power light pulses. However, owing to the limitations imposed by the source generation technology, amplification and propagation, beam quality control, and efficient harmonic conversion of low-coherence light pulses, the development of this field has faced great challenges. Several years ago, a brand-new scheme for achieving a low-coherence high-power laser driver was proposed in our institute. After several years of work, a kilojoule low-coherence laser driving facility has been successfully developed and has recently been put into service for experimental physics research. In the following sections, the progress made by our research team in key techniques, related theories, and verification of system integration will be described in detail.

III. GENERATION AND CONTROL OF INSTANTANEOUS BROADBAND LOW-COHERENCE PULSES

It is generally believed that broadband laser drivers have two main advantages compared with traditional high-coherence laser drivers (including various beam smoothing techniques): (1) larger output bandwidth—by increasing the bandwidth, it is possible to suppress the growth of parametric instability during laser–plasma interaction; (2) better smoothing of the focal spot—the larger the bandwidth and the more abundant the spectral components, the better is the integral smoothing effect. However, in recent years, there has been growing realization that relying on these two advantages alone is not enough to overcome the problems encountered in attempting to achieve ignition. For example, some efforts have been made to use broadband chirped pulses to suppress LPI, but the effects have been limited according to both theoretical simulations and experimental studies.[108]

In recent years, LPI studies have shown that the growth time of parametric saturation is of the order of picoseconds. For low-coherence light, if the spectral characteristics of the speckles and the time evolution characteristics of their spatial or longitudinal intensity distribution exhibit significant differences compared with those of traditional lasers on a picosecond time scale or the corresponding spatial length scale, then it could be possible to exploit these differences to suppress the effect of LPI. In addition to the broadband characteristic, two additional features need to be added to a broadband source to meet the above requirements: (1) instantaneous broadband characteristics, i.e., the spectral bandwidth on any sub-picosecond time scale should be equivalent to the integral spectral bandwidth of the entire pulse; (2) spectral incoherence, i.e., there should be no correlated and definite phase relationship among the spectral components. If a low-coherence beam with these characteristics is subjected to spatial smoothing, then, on the one hand, the broad spectral characteristics of an instantaneous broadband pulse are expected to delay the growth time of LPI, and, on the other hand, the sub-picosecond rapidly changing 3D distributed speckle field is expected to effectively cut off the path of LPI growth in the high-intensity region of the speckles. The combination of the above two requirements is expected not only to alleviate or even eliminate the problem of LPI, but also to greatly improve the smoothness of the focal spot.[42,109]

Figure 7 shows the beam characteristics that the brand new low-coherence pulse should have. Owing to the features of high coherence and narrow linewidth, the time–frequency diagram of traditional lasers is a single time-invariant spectral line, as shown in Fig. 7(a1). For a certain instant, the spectrum and phase are fixed and single, and there is a single isolated point on the frequency–phase diagram, as shown in Fig. 7(a2). The chirped pulse introduces second-order dispersion to broadband phase-locked light, i.e., the spectral components are linearly stretched in time. On the time–frequency diagram, there is a straight line whose frequency changes linearly with time [Fig. 7(b1)]. However, on a given instantaneous frequency–phase diagram, there is still a single point composed of a single spectrum and a single phase [Fig. 7(b2)]. In contrast to Fig. 7(a1), where the spectrum does not change, the frequency and phase of the chirped pulse change with time, and thus the positions are different. Different spectra of the transform-limited pulse propagate simultaneously because there is no residual dispersion. Therefore, at a given time, all frequencies of the transform-limited pulse have the same phase, i.e., there is a flat line on the frequency–phase diagram, as shown in Figs. 7(b1) and 7(b2). The time–frequency characteristic of a phase-modulated pulse obtained by the SSD technique is shown in Fig. 7(c1). The SSD technique sweeps the spectrum of the phase-modulated pulse periodically, and so isolated frequencies have different phases at a given time, as shown in Fig. 7(c2). Unlike the above-mentioned pulses, the frequencies of an instantaneous broadband pulse are broadband and plentiful at any instant of time, similar to the effect of "white light," as shown in Fig. 7(d1). Moreover, different spectra have no fixed phase relationship [Fig. 7(d2)]. Pulses with this unique property have lower coherence, and may be used to suppress LPI and effectively improve the uniformity of the focal spot.

From a review of the discussion of various types of low-coherence sources in Sec. II, it can be seen that none of these sources can simultaneously possess the characteristics of Figs. 7(d1) and 7(d2) (i.e., instantaneous broadband low coherence). The closest is the ASE source used by Gekko XII. However, owing to the limitation of its generation method, its spectral width is narrow and its spectral coherence is too high. Not only are the physical effects that can be achieved limited, but also the temporal characteristics of the pulse are severely affected, resulting in the limitations on the ouptput of the facility under conditions of high fluence and high intensity.

Aiming at low-coherence pulses with instantaneous broadband characteristics, two kinds of sources are introduced in the front-end system of our low-coherence laser facility: a superluminescent diode (SLD) source (a source with low temporal coherence and high spatial coherence) and a thermal light source (a source with low temporal coherence and low spatial coherence). The thermal light source is still under development, and so the results described in this article are based on the SLD source. The SLD is a diode light source that produces emission via electron–hole recombination across the bandgap.[110] In contrast to a traditional laser diode (LD), an SLD has no resonant cavity, and its emitter facets are antireflection-coated and tilted to suppress lasing

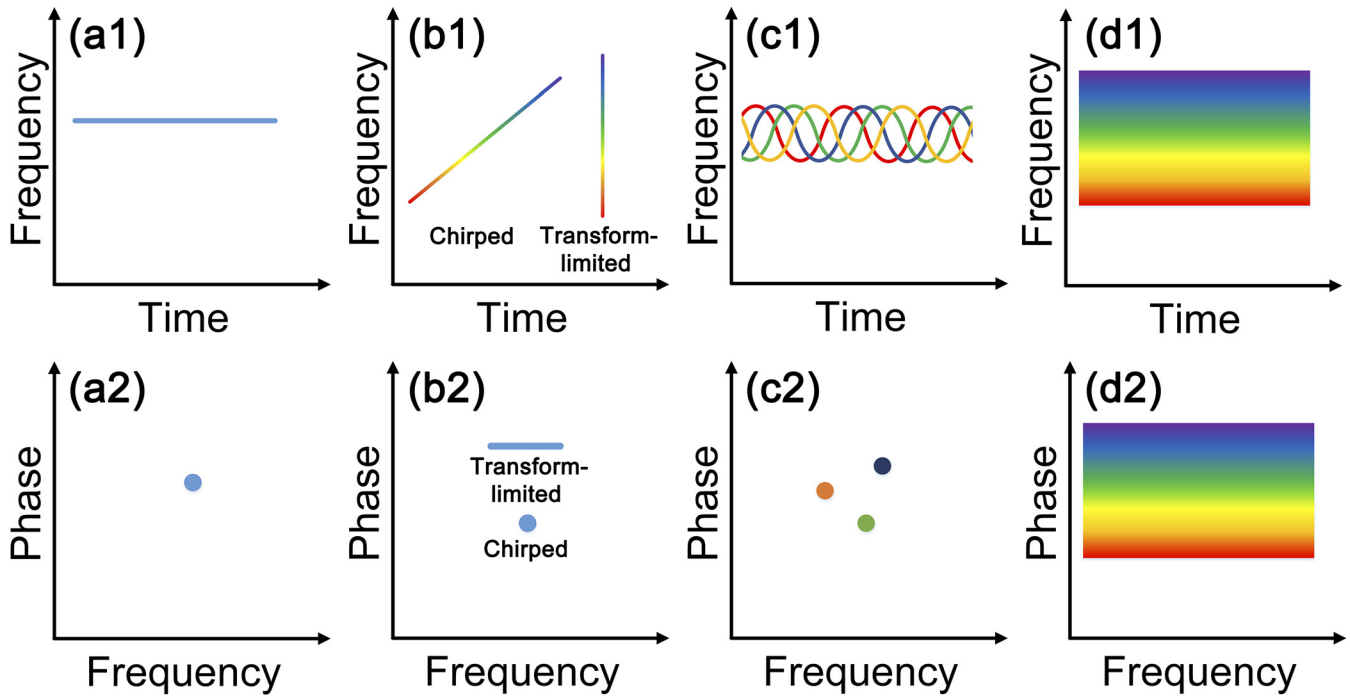

FIG. 7. Optical frequency as a function of time for different light sources: (a1) high-coherence pulse; (b1) chirped pulse and transform-limited pulse; (c1) phase-modulated pulse; (d1) instantaneous broadband pulse. (a2), (b2), (c2), and (d2) are the corresponding frequency–phase diagrams.

oscillation inside,[111,112] leading to a smooth output spectrum free of any longitudinal modes. This type of source has extremely rich spectral components with very little phase correlation, so it has extremely low temporal coherence.

A schematic of the low-coherence front-end system is shown in Fig. 8.[43] The seed source is an SLD with an output center wavelength of 1050 nm, a bandwidth of 50 nm, and a continuous power of 8 mW. A waveguide amplitude modulator is used to vary the intensity of the light in response to an arbitrary waveform generator. The low-coherence light is chopped into 3-ns pulses with a 1-kHz repetition rate. The pulses are amplified by two-stage single-mode double-pass Yb-doped fiber amplifiers. The pulses are then collimated to a spectral control module consisting of a half-wave plate, two polarizers, and a birefringent crystal to vary the spectral distribution. Finally, the pulses are amplified to 1 μJ through a double-clad Yb-doped fiber amplifier.

The pulse shape can be precisely modulated through the amplitude modulator. The graphs in Fig. 9 show different characteristic examples of temporal profiles of laser impulses. The rise time of the pulse can be less than 200 ps and the contrast ratio is greater than 130:1. Figure 9(d) demonstrates the spectra of different pulse shapes from which it can be seen that the spectrum remains highly consistent as the pulse temporal profile varies, which is quite different from traditional broadband pulses (phase-modulated pulses and chirped pulses).

Not only can the temporal profile be arbitrarily shaped, but also the spectrum can be precisely controlled for special applications. Figures 10(a)–10(c) show different spectra modulated through the spectral control module. The spectra after amplification maintain their continuous and smooth characteristics (without longitudinal mode structure or spectral beat frequency), which is beneficial for achieving better beam smoothing effects. As displayed in Fig. 10(d), when the spectrum is shaped over a wide range, the temporal profile of the pulse exhibits no obvious change due to the loss of spectral components in a large region. Thus, the pulses obtained exhibit the characteristics of instantaneous broadband pulses: the frequencies of the pulse at any time are broadband and plentiful, which is very beneficial for improving the result and speed of smoothing.

Coherence length or coherence time is often used to describe the temporal coherence of a pulse, since these can be measured experimentally with a Michelson interferometer. The measured coherence length of the output pulse is about 37 μm, corresponding to a coherence time of 123 fs, which is much shorter than the pulse duration. Therefore, the low-coherence pulses that we obtain can achieve a much shorter smoothing time than traditional laser pulses. Moreover, the output energy shows excellent stability, with less than 1% rms instability and 8% peak-to-valley instability over 4 h, which is very beneficial to improving the performance of the laser facility.

Compared with previous low-coherence sources, the set of low-coherence sources that we have developed not only have the instantaneous broadband and spectral incoherence characteristics exemplified by Figs. 7(d1) and 7(d2), but also realize the high-contrast

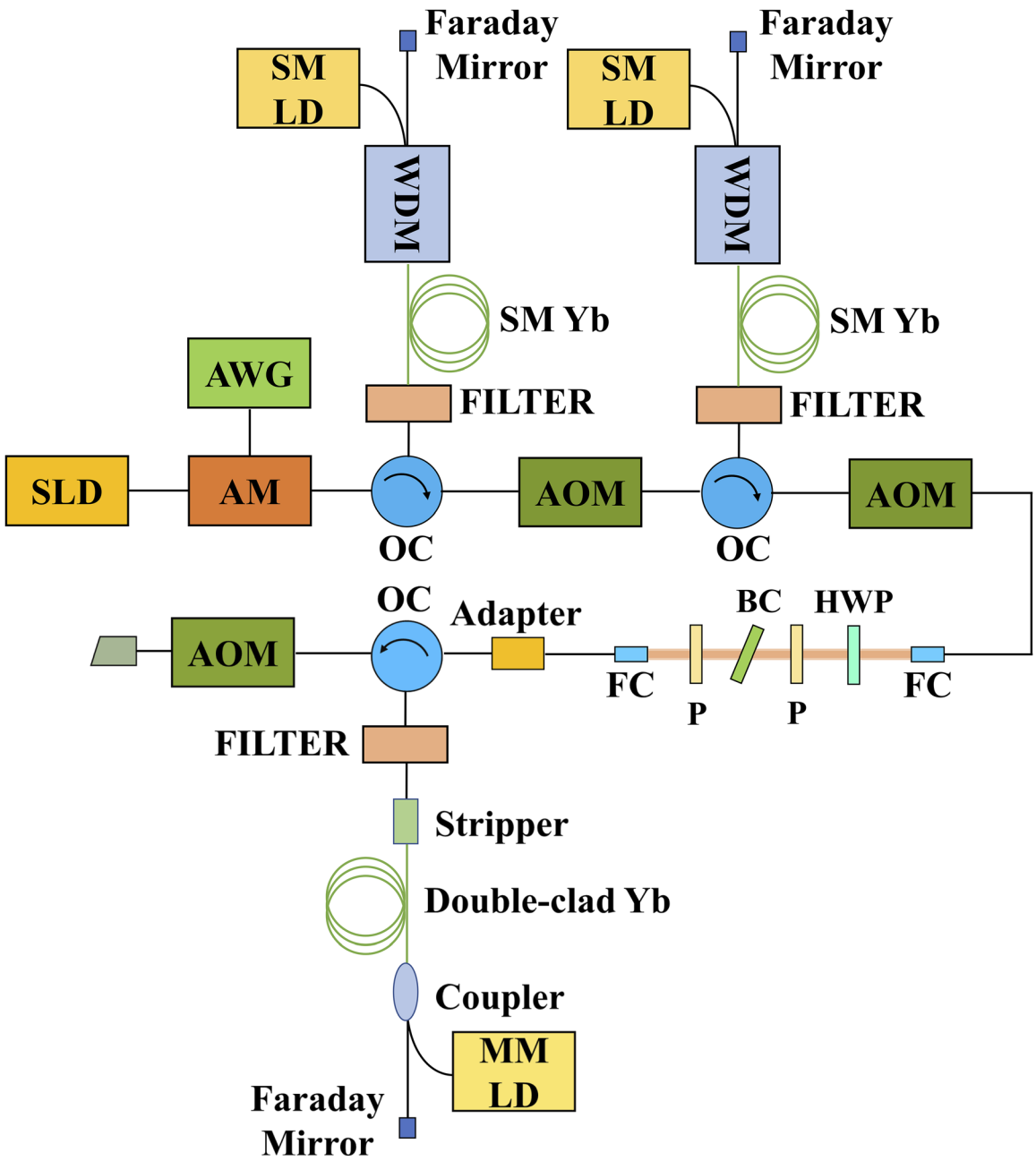

FIG. 8. Schematic of the low-coherence front-end system. AWG, arbitrary waveform generator; AM, amplitude modulator; OC, optical circulator; SM LD, single-mode laser diode; WDM, wavelength division multiplexer; AOM, acoustic optical modulator; FC, fiber collimator; M, mirror; HWP, half-wave plate; P, polarizer; BC, birefringent crystal; MMLD, multimode laser diode. Reprinted with permission from Rao *et al.*, Opt. Laser Technol. **122**, 105850 (2020). Copyright 2020 Elsevier.

precise time-shaping capability required by future precision physical experiments with low-coherence drivers and the spectral-shaping capability required by the subsequent broadband low-coherence amplification process. In addition, this type of source has been developed based on a single-mode polarization-maintaining optical fiber, which can provide a good match with a traditional high-power amplifier chain. This maximizes the possibility of sharing key techniques and system integration with traditional ICF drivers. Meanwhile, the use of low-coherence laser drivers allows experimental research into laser–plasma interaction, absorption, and smoothing effects on targets to be carried out at the lowest cost and highest speed.

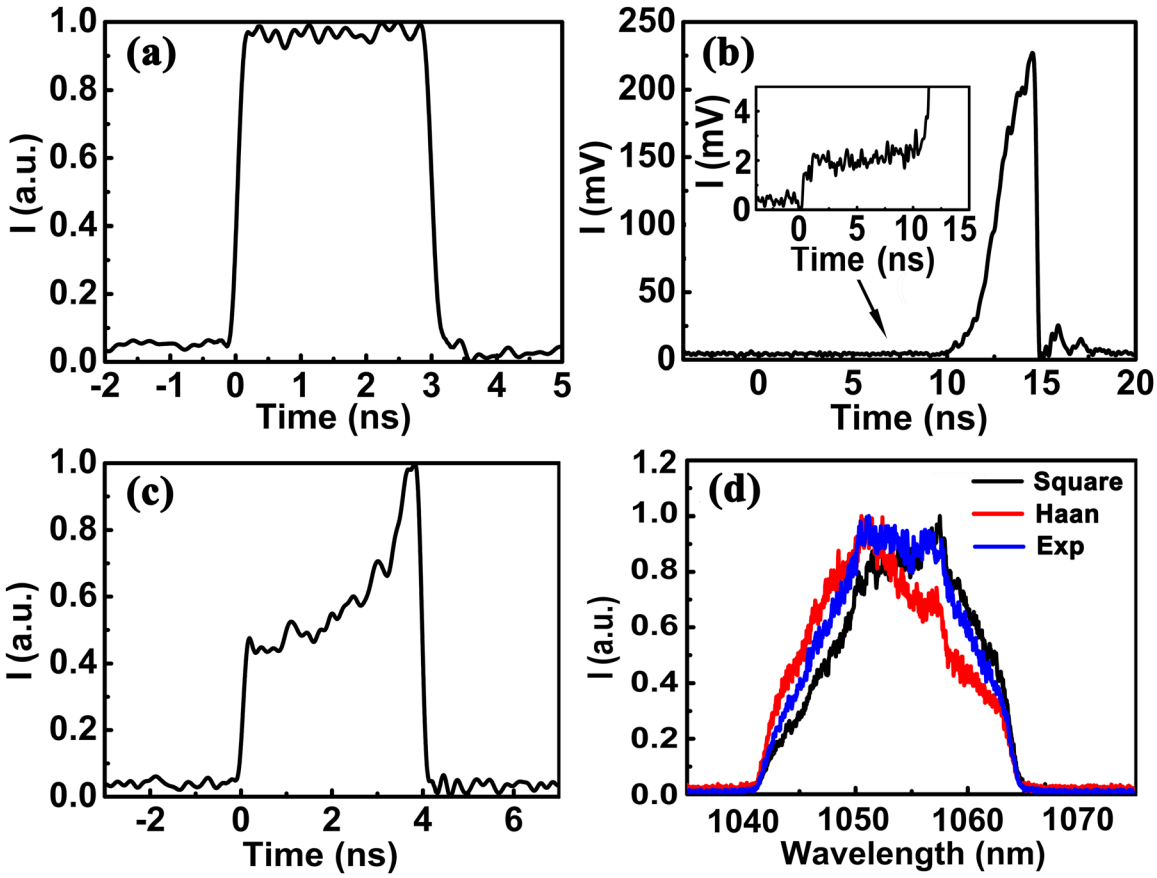

FIG. 9. Illustration of the pulse shapes that can be generated by our system: (a) square pulse; (b) high-contrast pulse; (c) exponential pulse; (d) spectra of different pulse shapes. Reprinted with permission from Rao *et al.*, Opt. Laser Technol. **122**, 105850 (2020). Copyright 2020 Elsevier.

IV. BROADBAND AMPLIFICATION OF LOW-COHERENCE PULSE

The amplification of low-coherence light pulses in Nd:glass systems faces two major problems: how to obtain a sufficiently large bandwidth to ensure the required low coherence and how to securely and efficiently obtain sufficiently high energy. In the past, the bandwidths of kilojoule-level laser amplifiers (pure Nd:glass systems) were limited to a few nanometers (~2 nm). At the beginning of our project, the goal of an output bandwidth greater than 10 nm was set. Even for amplification of coherent lasers, there is currently, no facility based on a pure Nd:glass system that can amplify microjoule-level pulses to the kilojoule level at a bandwidth greater than 2 nm. A three-level spectral control strategy has been adopted to achieve this goal: the front-end spectrum is precisely adjustable, the high-gain section maintains flat-top gain, and the large energy section is pre-compensated to ensure a high enough spectral gain. To maximize the spectral incoherence of the low-coherence source, components with mode-selection effects are avoided as far as possible in the design of the amplifier. In the past, low-coherence drivers with large energy output were often confronted with two major risks: damage caused by temporal modulation and insufficient gain capability. To overcome these hazards, on the one hand, any component that may increase spectral coherence is comprehensively avoided in the whole system design, and, on the other hand, the gain capability margin is increased moderately in the high-gain section. Based on these principles, the amplifier chain consists of two portions: a high-gain preamplifier and a high-energy main amplifier. Various control methods have been optimally configured according to their respective characteristics.

A. High-gain preamplifier

A schematic of the preamplifier is shown in Fig. 11.[44] The front end with an output energy of ~1 μJ and a spectral width of 25 nm is connected into the preamplifier system, whose gain medium is Nd-doped phosphate glass (type N31, with different Nd^{3+} ion concentrations at different stages). The preamplifier chain contains two main stages: a repetitive amplifier and a single-shot amplifier (one shot in 15 min). In the repetitive amplifier stage, a Pockels cell is used to pick pulses at 1 Hz. The gain media are 3-mm-diameter rods and 8-mm-diameter rods pumped by laser diodes and xenon flashlamps, respectively. An optically addressed liquid crystal spatial modulator is used for near-field pulse shaping (10×10 mm^2) and compensation of

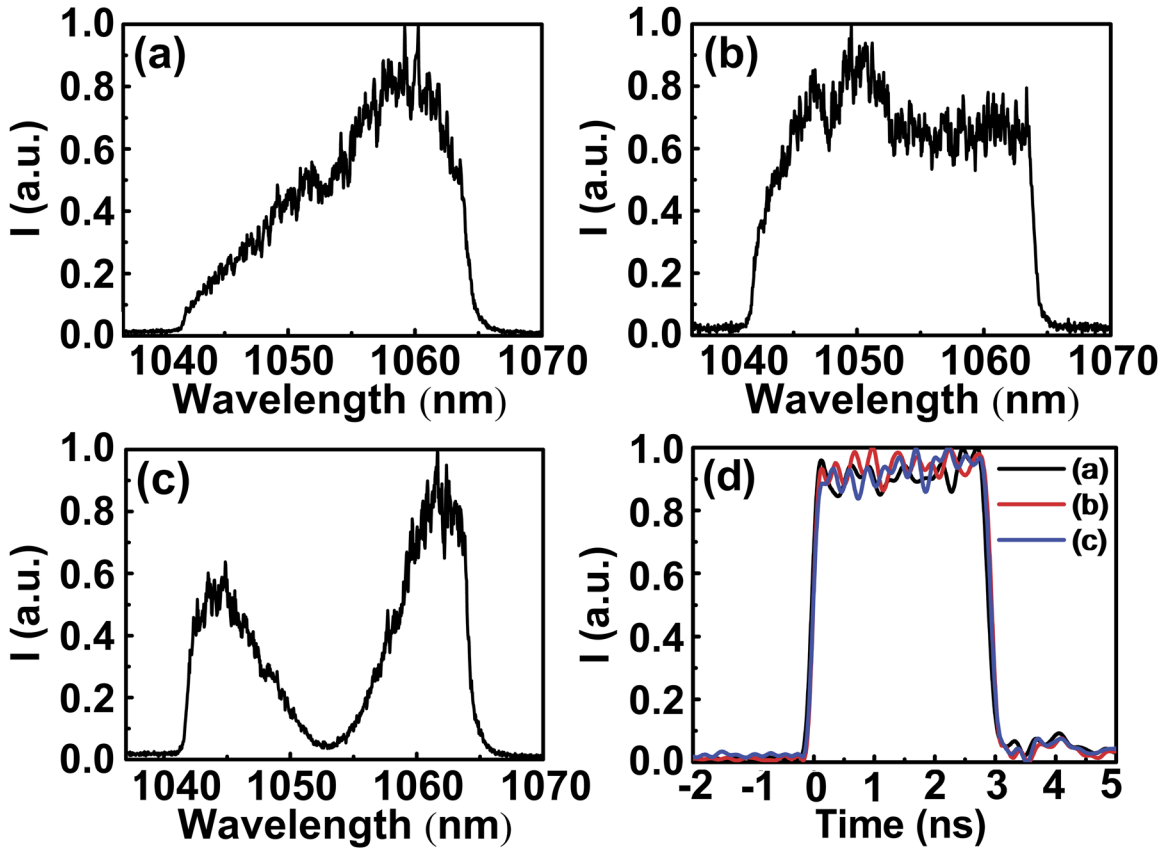

FIG. 10. (a) Spectrum without spectral control. (b) Spectrum with a nearly flat top. (c) Saddle-type spectrum for a Nd:glass amplifier. (d) Temporal profiles of the spectra in (a)–(c). Reprinted with permission from Rao *et al.*, Opt. Laser Technol. **122**, 105850 (2020). Copyright 2020 Elsevier.

the spatially non-uniform gain profiles of the amplifiers. In the single-shot amplifier stage, a 20-mm-diameter rod, three 40-mm-diameter rods, and three 70-mm-diameter rods cooled by pure water act as energy amplifiers. An electro-optical switch is used for suppression of ASE. The beam size at the output of the preamplifier is 42×42 mm^2.

However, high-gain and high-energy amplification in a Nd:glass amplifier chain is always accompanied by a spectral gain narrowing effect. To restrain the spectral narrowing effect of our laser system, four spectral shaping filters are inserted into the preamplifier chain at locations near the 3-mm, 20-mm, and 40-mm rods. Each of the birefringent filters consists of a 4-mm-thick quartz crystal combined with two polarizers. Both the central wavelength and the transmission depth can be tuned by adjusting the tilt and rotation of the quartz crystal. The response shapes of the birefringent filters are designed to match the inverse gain shapes of different amplification processes. The output energy of the repetitive amplifier is 157 μJ at a 1-Hz repetition rate, and the preamplifier section produces an output energy of 35 J.

In the preamplifier section, the broad spectral profile of the pulse with 5-ns square waveform is shown in green in Fig. 12(b). When the temporal shape is tailored to a 3-ns square wave, the spectral shape remains unchanged (green and red profiles in Fig. 12), proving that its spectral composition is not significantly associated with time. This is completely different from the chirped broadband pulse. When the spectrum of the 3-ns square wave is greatly adjusted to the shape of a saddle, to meet the spectral compensation requirement for downstream amplification, the temporal shape remains nearly unchanged, in spite of the loss of spectral components over a large range (red and blue profiles in Fig. 12). This phenomenon further indicates that the distribution of spectral components is time-independent. These results reveal that the instantaneous broadband property of the pulse is not changed during the process of amplification.

A shorter coherence time of the output pulse leads to a greater improvement in the suppression of LPI during laser fusion. Typical pulse coherence characteristics in the front end, repetitive amplifier, and single-shot amplifier are illustrated in Fig. 13. The dots are experimental results and the curves are optimum fitting curves obtained by using a sinc function because of the nearly flat-topped spectral shape. The temporal coherence increases at the repetitive amplifier output owing to the narrowing of the spectral width compared with that of the front end [green and red curves in Fig. 13(b)]. As high-gain amplification proceeds, the coherence time increases slightly because of the small decrease in spectral width from 11.4 nm to 10.2 nm [red and blue curves in Fig. 13(b)]. The measured coherence time of the instantaneous broadband laser at the output of the single-shot amplifier is ~318 fs. The coherence time of the instantaneous broadband

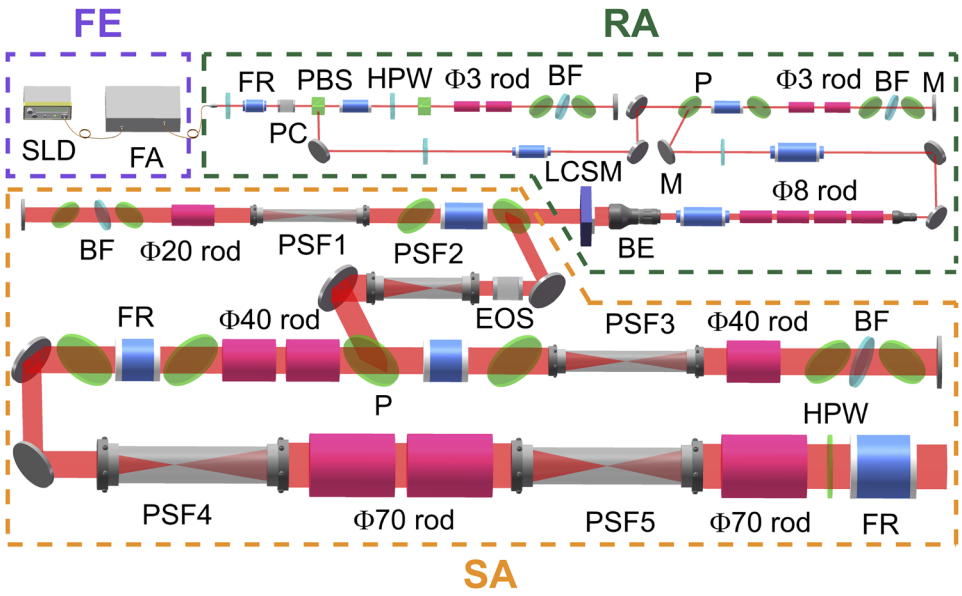

FIG. 11. Schematic of the high-gain preamplifier: FE, front end; RA, repetitive amplifier; SA, single-shot amplifier; FA, fiber amplifier; HWP, half-wave plate; FR, Faraday rotator; PC, Pockels cell; PBS, polarizing beam splitter; BF, birefringent filter; P, polarizer; M, mirror; BE, beam expander; LCSM, liquid crystal spatial modulator; PSF, spatial filter; Φ, Nd:glass rod (diameter, mm); EOS, electro-optical switch. Reprinted with permission from Cui *et al.*, Opt. Lett. **44**(11), 2859–2862 (2019). Copyright 2019 Optical Society of America.

light at the preamplifier output is far less than the pulse duration. As shown in Figs. 12 and 13, the instantaneous broadband and low-temporal-coherence characteristics of a light pulse in the system can be maintained after amplification by more than 10^7 times, which is exactly what is needed by laser drivers.

B. High-energy main amplifier

The basic design principle of the main amplification subsystem is to match the requirements of maximum energy output (large energy gain and extraction) with minimal technical difficulties and implementation costs. An optical schematic of the main amplifier chain is shown in Fig. 14. In the main amplifier section, six Nd-doped phosphate glass (type N31) disk amplifiers with a clear aperture of 400×400 mm^2 are arranged in sequence and all of them are placed at the Brewster angle.[50] To reduce the complexity of the system and avoid the need to design a large-aperture amplifier step by step, a multipass (five-pass) amplification scheme pumped by xenon flashlamps is adopted. The output beam of the preamplifier subsystem is expanded to 160×160 mm^2 by spatial filter 1. The beam size is chosen for the purpose of achieving multipass amplification in the near-field mode and to avoid the use of large-aperture electro-optical switches or beam inverters. The amplified beam is then relay-imaged by spatial filter 2 to the nonlinear crystal for harmonic conversion.

To acquire a nearly flat-top spectrum at the output of the main amplifier, the spectrum of the preamplifier output in the laser system is over-compensated. The amplifier chain produces an output spectrum with a bandwidth of 13 nm,[50] as shown in Fig. 15. The output energy of the main amplifier is more than 1 kJ, with a 3-ns pulse duration (Fig. 16). Under high-energy conditions, low-

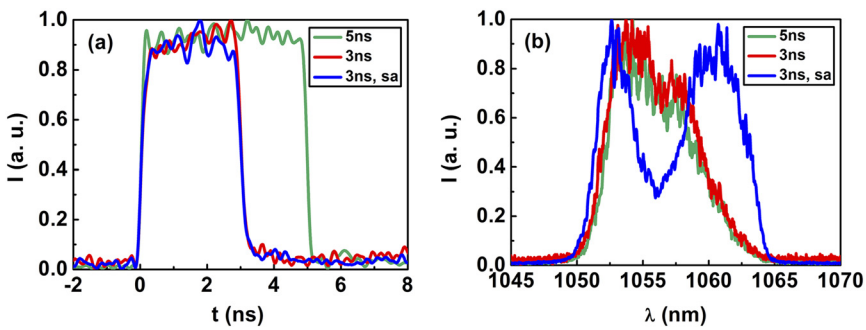

FIG. 12. (a) Temporal and (b) spectral profiles of the light in the single-shot amplifier. The "sa" label indicates the saddle-shaped spectrum. Reprinted with permission from Cui *et al.*, Opt. Lett. **44**(11), 2859–2862 (2019). Copyright 2019 Optical Society of America.

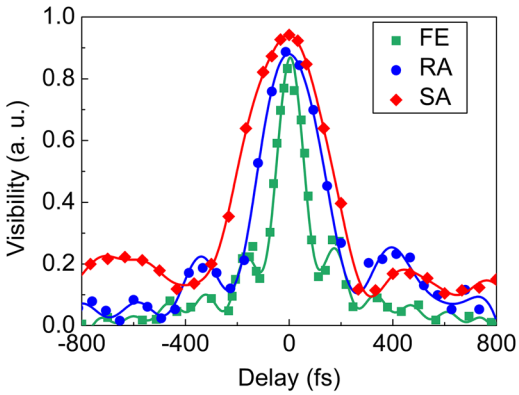

FIG. 13. Visibility of interference fringes at different locations. The dots are experimental results, and the curves are fitting results. FE, front end, RA, repetitive amplifier, SA, single-shot amplifier. Reprinted with permission from Cui *et al.*, Opt. Lett. **44**(11), 2859–2862 (2019). Copyright 2019 Optical Society of America.

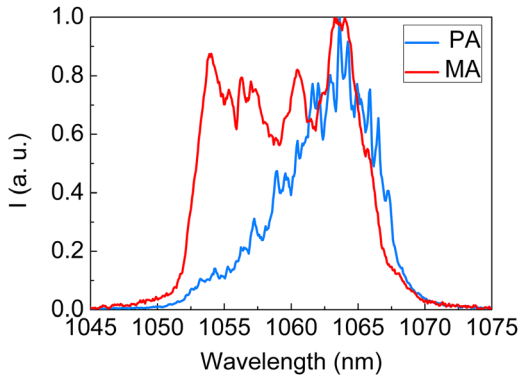

FIG. 15. Spectra of preamplifier and main amplifier.

temporal-coherence broadband pulses with good spatial uniformity and focusing capability are especially important for maximizing the output energy and controlling the intensity in the target plane of a laser driver system. Near-field and far-field images of the output pulse in the main amplifier section are presented in Fig. 17. The aperture fill factor (defined as the ratio of the average light intensity to the maximum light intensity within the zero-intensity aperture of the beam) of the spatial profile is 0.75, and the fluence beam contrast (defined as the rms value of the fluctuation of the spatial intensity distribution in the near-field flat-top area of the beam, i.e., within 70% of the zero-intensity aperture) is 0.093. Figure 17(b) shows the far-field profile of the beam, in which more than 95% of the energy is in the range of eight times the diffraction limit, confirming the good far-field performance and revealing the low-temporal-coherence and high-spatial-coherence characteristics of the amplified pulse.

Key results such as 1000-J pulse energy, 13-nm bandwidth, 280-fs coherence time, 5-J/cm^2 output fluence, 1.7-GW/cm^2 intensity, and hundreds of safe shots under these conditions (since the installation of the facility, no component damage caused by the strong laser has been found) indicate the appropriateness and effectiveness of the design and control technology adopted by the system. The above results provide very valuable basic data and research experience for the design and development of this type of facility in the future.

V. EFFICIENT FREQUENCY CONVERSION OF LOW-COHERENCE LIGHT

The frequency conversion efficiency is one of the primary factors limiting the final output capability of low-coherence laser devices. However, the results reported from low-coherence laser facilities (see Sec. II) show that at present, the conversion efficiency is significantly lower than that for high-coherence lasers, and the bandwidth of harmonic waves is still insufficient for laser driver applications. To increase efficiency, the theoretical understanding of frequency conversion needs to be improved by considering the low-coherence characteristics of the fundamental wave, and a suitable phase matching scheme needs to be developed.[46]

The output low-coherence pulses of our laser facility have instantaneous broadband characteristics, i.e., the frequency components have a wide distribution at any time within the pulse duration.[44] The analysis earlier in this paper shows that the output pulses satisfy the statistical properties of polarized thermal light. Their amplitude and phase are statistically independent. The phase is uncorrelated

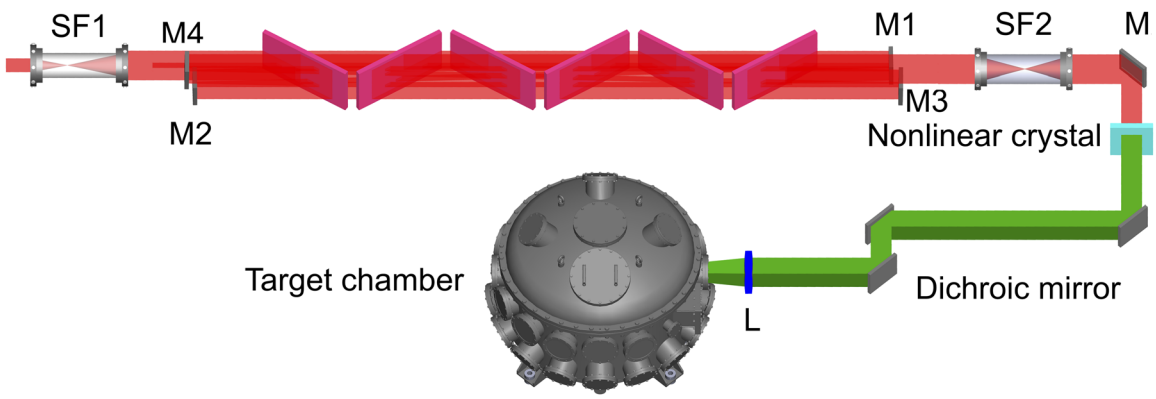

FIG. 14. Schematic layout of the main amplifier. SF, spatial filter, M, mirror, L, lens.

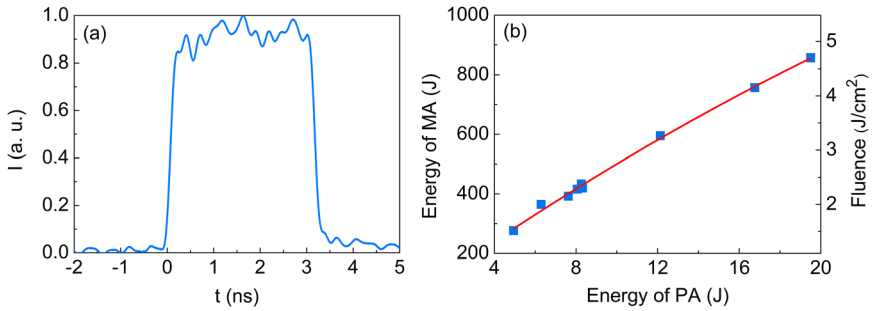

FIG. 16. (a) Temporal profile and (b) output energy of main amplifier.

between different frequencies and uniformly distributed in the whole range of $[-\pi, \pi]$. Thus, the frequency conversion characteristics of these low-coherence pulses should be analyzed using the methods of statistical optics.

A. Theoretical analysis

For the fundamental wave, the electric field of the low-coherence pulse at a central frequency ω_0 can be expressed as a Fourier transform, under the assumption that it propagates along the z axis:

$$E_1(z,t) = \frac{1}{2}\left[\frac{1}{2\pi}\int_0^{+\infty} \varepsilon_1(z,\omega)e^{i[\omega t - k_1(\omega)z]}d\omega + c.c.\right], \tag{5}$$

where $\varepsilon_1(z, \omega)$ is the complex frequency-domain pulse field, ω is the angular frequency, and $k_1(\omega)$ is the wave vector.

By solving the nonlinear coupled equations and making the slowly varying envelope approximation and the small-signal approximation, the complex frequency-domain field of the second-harmonic wave at the output of the nonlinear crystal is obtained as

$$\varepsilon_2(L,\Omega) = -\frac{i\omega_0 d_{\text{eff}}}{n_2 c}\int_0^{+\infty}\frac{d\omega}{2\pi}\varepsilon_1(z,\omega)\varepsilon_1(z,\Omega-\omega) \times L\exp\left(\frac{i\Delta L}{2}\right)\text{sinc}\left(\frac{\Delta L}{2}\right), \tag{6}$$

where L is the thickness of the nonlinear crystal, Ω is the angular frequency of the second harmonic, and n_2 is the refractive index of the second harmonic. The phase mismatch $\Delta k = k_2(\Omega) - k_1(\omega) - k_1(\Omega - \omega)$, where $k_2(\Omega)$ is the wave vector of the second harmonic.

Equation (6) indicates that the SHG process of these pulses contains not only the degenerate SHG of each frequency component but also the sum-frequency generation of different frequency components of the pulses, which is different from that of modulated pulses and chirped pulses. To analyze the spectral distribution of the second harmonic, the statistical properties of the fundamental wave should be considered. Statistical optics is introduced to calculate the power spectral density (PSD):

$$g(\Omega) = \langle \varepsilon_2(\Omega)^* \varepsilon_2(\Omega)\rangle = \left(\frac{\omega_0 d_{\text{eff}}}{2\pi n_2 c}\right)^2 |H(\Omega)|^2 S(\omega) \otimes S(\omega), \tag{7}$$

where $\langle\cdots\rangle$ denotes the average over infinite time, $|H(\Omega)|^2 = L^2\,\text{sinc}^2(\Delta kL/2)$ describes the filtering effect caused by phase mismatching, and $S(\omega)$ is the PSD of the fundamental wave. From Eq. (7), we can conclude that all the frequency components of the fundamental wave are involved in the harmonic conversion process, and the spectrum of the second harmonic is proportional to the self-convolution of that of the fundamental wave. This differs from coherent nonlinear processes, in which the convolution relationship is between the frequency-domain electric fields of the second-harmonic and fundamental waves.

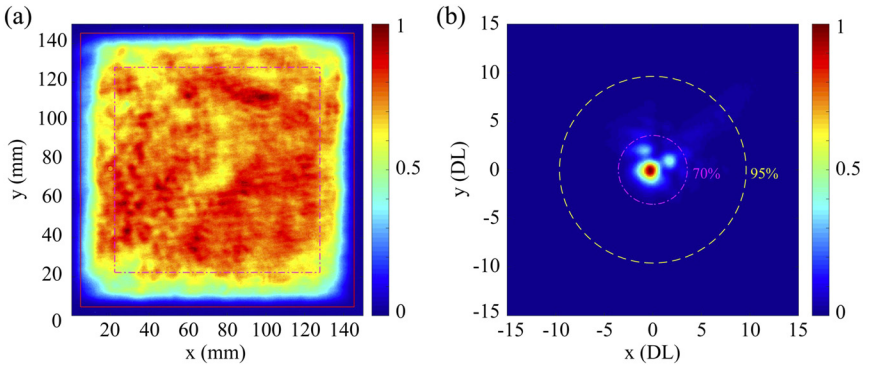

FIG. 17. (a) Near-field pattern and (b) far-field profile in the main amplifier section.

Furthermore, the spectral bandwidth of the second harmonic is also partially determined by the filtering function $|H(\Omega)|^2$. To achieve a broadband frequency conversion process, the phase mismatch Δk should be kept to zero over the whole frequency range. When phase matching at the central wavelength is satisfied, the phase mismatch in the second-order approximation is $\Delta k = \Delta(v_g^{-1})(\Omega - 2\omega_0)$, where $\Delta(v_g^{-1})$ corresponds to the group-velocity mismatch. Therefore, simultaneously satisfying the phase-matching and group-velocity-matching conditions is the key factor for broadband low-coherence frequency conversion.

The nonlinear crystal delivers low-coherence pulses with a bandwidth of up to 15 nm. For such a broadband nonlinear process, the use of a nonlinear crystal operating at the retracing point of phase matching is a simple and implementable scheme that can satisfy the phase-matching and group-velocity-matching conditions simultaneously. In Nd:glass laser systems, KDP crystals are usually used for SHG. Nevertheless, the retracing point of phase matching is then 1034 nm, which is far from the central wavelength of the laser (1057 nm). The refractive index of the KDP crystal can be changed by partial deuterium doping, thereby moving the retracing point of phase-matching. According to theoretical calculations, 15%-deuterated KDP crystals can move the retracing point to 1057 nm, allowing a broadband SHG process. By utilizing a 15% DKDP crystal operating at the retracing point of phase matching, efficient and broadband SHG can be achieved.

B. Phase matching at the retracing point of a partially deuterated KDP crystal

While waiting for a large-diameter 15% DKDP crystal to be prepared, we have conducted preliminary experiments at the output of the high-gain preamplifier.[45] The spatial profile of the fundamental wave is close to a 12th-order super-Gaussian with a size of 42×42 mm^2. It delivers an energy up to 30 J within a 3-ns pulse duration. The spectrum has a rectangular distribution with a bandwidth of ~10 nm and centered at 1057 nm. A type I 15% DKDP crystal with a cutting angle of 41° is utilized as the nonlinear crystal. The size of the crystal is $70 \times 70 \times 32$ mm^3. The central phase-matching wavelength is 1057 nm, with an acceptance bandwidth of about 12 nm.

The experimental results for SHG are shown in Fig. 18. The time waveform of the second harmonic is square, with a pulse duration of 3 ns, which is the same as that of the fundamental wave [Fig. 18(a)]. Consistent with the theoretical prediction, the spectrum of the second harmonic with a triangular shape is the self-convolution of the fundamental wave spectrum [Fig. 18(b)]. All of the spectral components have participated in the frequency-conversion process. The conversion efficiency is up to 70%, with a bandwidth of 2.9 nm (3.1 THz at 527 nm). To the best of our knowledge, this is the broadest bandwidth and highest conversion efficiency of low-coherence SHG to date. The curve in Fig. 18(c) is the simulation result based on the theoretical analysis presented above. The simulation and experimental results are in good agreement with each other. Theoretically,

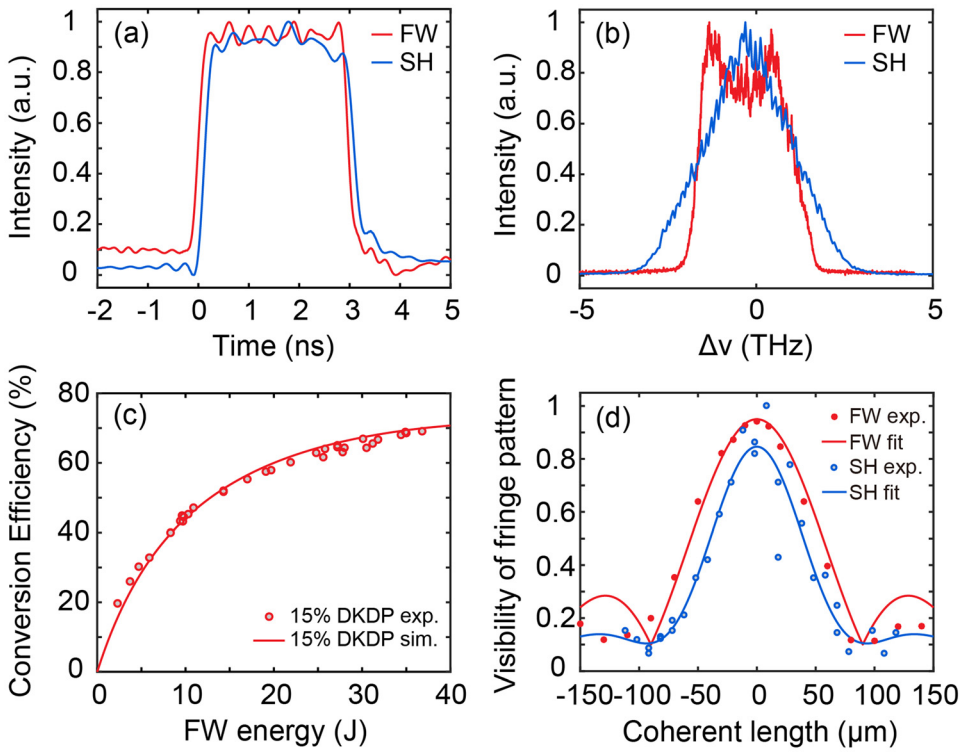

FIG. 18. Results of SHG in the low-coherence laser facility. Reprinted with permission from Ji *et al.*, Opt. Lett. **44**(17), 4359–4362 (2019). Copyright 2019 Optical Society of America.

the conversion efficiency will be up to 80% with an incident fundamental wave power density of 3 GW/cm^2–4 GW/cm^2, which is the same as the highest conversion efficiency on conventional coherent laser facilities for ICF.

The coherent characteristics are retained in the SHG, since the temporal coherence lengths of the fundamental wave and the second harmonic are almost the same, corresponding to a coherence time of 300 fs [Fig. 18(d)]. This demonstrates the second-harmonic output capability of the preamplifier. Near-field and far-field focusing characteristics of the fundamental wave and the second harmonic are also investigated, as shown in Fig. 19. The second-harmonic pulse retains good near-field quality (with a flux contrast of 0.228) and excellent far-field performance (95% energy within 3.7 times the diffraction limit). This represents the good focusing capability required for practical applications.

C. Single KDP crystal

As there is some uncertainty regarding when the large-diameter 15% DKDP crystal will be available, an experimental study of SHG utilizing a KDP crystal has been carried out at the output of the preamplifier, with the aim of realizing high-energy low-coherence second-harmonic output as soon as possible. It is arranged for type I phase matching with a cutting angle of 41°, and the crystal has the same size as the 15% DKDP crystal used at the output of the preamplifier. The acceptance bandwidth of the second-harmonic wave is 2 nm. With the same fundamental-wave conditions as in the SHG experiments with a 15% DKDP crystal described in Sec. V B, the experimental and simulated results are shown in Fig. 20. The highest conversion efficiency is about 55%, and the spectrum also has a triangular shape with a FWHM of 2 nm. Generally, the conversion efficiency of KDP crystals for broadband pulses is low. The conversion efficiency of low-coherence pulses in our experiments is up to 55%. This result exceeded our expectations, indicating that even a single KDP crystal can give good results. Although second-harmonic efficiency and bandwidth are slightly reduced, they are much higher than expected. This result can be understood in the context of the theory of SHG of low-coherence light proposed in Sec. V A. There is not only degenerate SHG of the same frequency component, but also self-pairing sum-frequency generation of different frequency

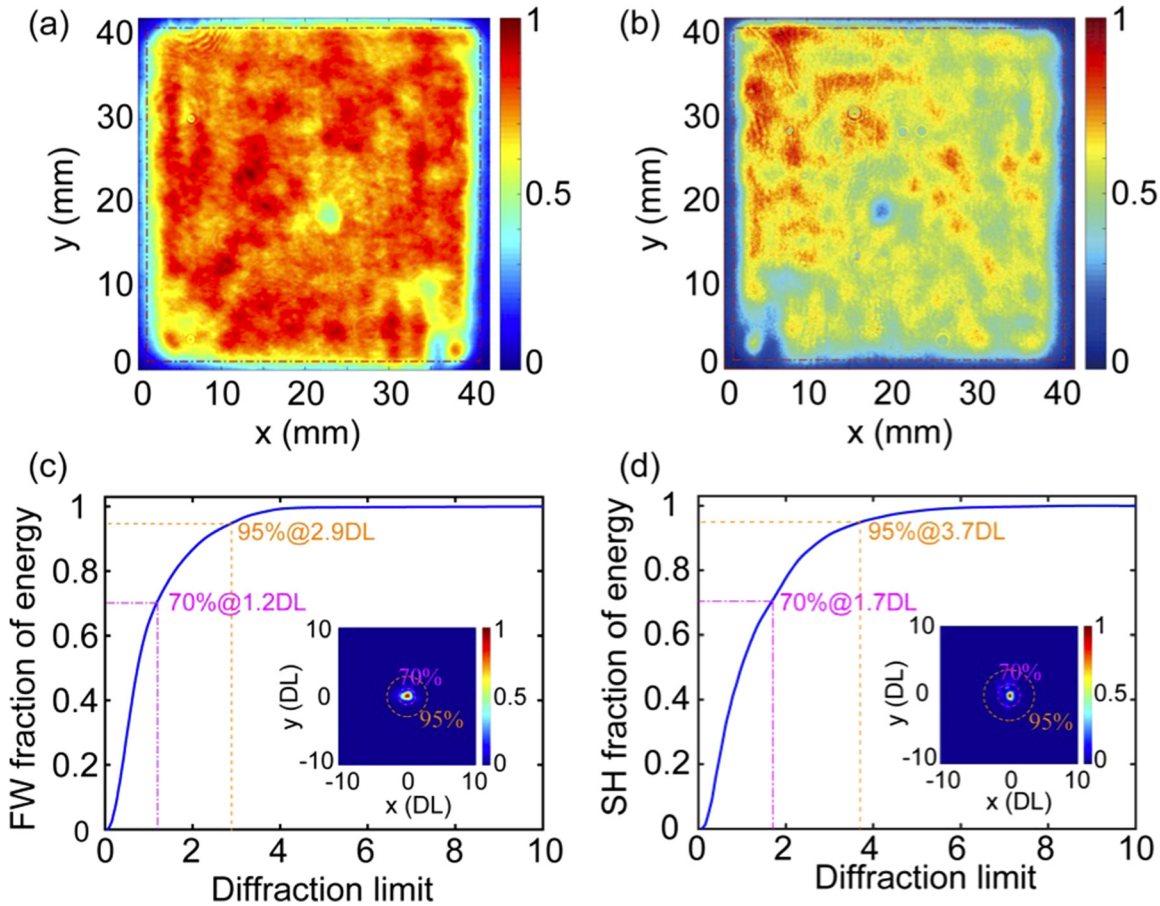

FIG. 19. Near fields of the fundamental wave (a) and the second harmonic (b), and the corresponding far fields of the fundamental wave (c) and the second harmonic (d). (a) and (c) are reprinted with permission from Cui *et al.*, Opt. Lett. **44**(11), 2859–2862 (2019). Copyright 2019 Optical Society of America. (b) and (d) are reprinted with permission from Ji *et al.*, Opt. Lett. **44**(17), 4359–4362 (2019). Copyright 2019 Optical Society of America.

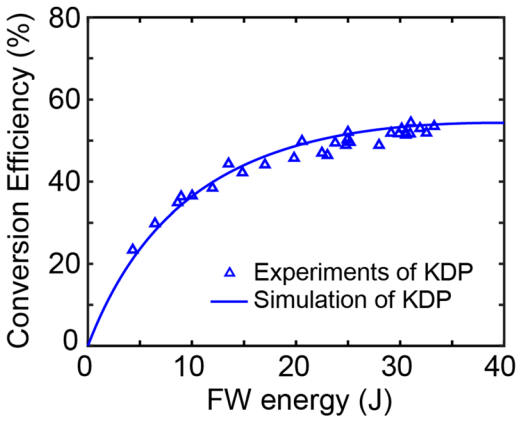

FIG. 20. Experimental and simulation results for second-harmonic efficiency vs fundamental wave energy when a KDP crystal is used.

components. Although the KDP crystal filters out the sideband components of the second harmonic, the remaining components are produced by sum-frequency generation from all frequency components. Sum-frequency generation processes play an important role in improving efficiency. Since the frequency components outside the filter function are mixed into the filter function again through sum-frequency generation processes, the overall harmonic conversion efficiency is improved. Following the achievement of kilojoule output of the fundamental wave, experiments on SHG utilizing a large-diameter KDP crystal ($200 \times 200 \times 24$ mm^3) have been carried out to realize high-energy second-harmonic output. Recently, we have completed SHG experiments using the large-diameter KDP crystal at the output of the main amplifier, achieving a second-harmonic output of 500 J with 3-ns pulse duration and a bandwidth of 2 nm. There is no significant degradation in near-field or far-field qualities.

We have obtained pieces of 200×200 mm^2 large-diameter low-deuterium-doped KDP crystals by two growth methods: a fast-growth method, which is being tested online, and the traditional method, which is being done offline.

D. Temporal characteristics

According to the results of research on pulse shaping,[113–115] finite temporal incoherence (i.e., incoherent bandwidth) may induce rapid intensity modulation. To further study the time characteristics of low-coherence pulses, we have measured the temporal profiles of second-harmonic pulses of this kind of pulse using a streak camera. The experimental conditions and parameters are similar to those of the SHG experiments with a large-diameter KDP crystal described in Sec. V C. Figure 21 shows the temporal intensity distribution of the second-harmonic conversion pulse. In a 2-ns time window, the resolution is ~11 ps. These results show that there is no serious white noise in the time domain within the resolution of the streak camera. The weak intensity fluctuations pose little risk to safe operation of the facility.

The establishment of a spectral conversion model for instantaneous broadband low-coherence pulses and the improvements in the associated theory bring new hope for the development of low-coherence drivers. The demonstration of frequency-doubling of low-coherence large-bandwidth pulses with an efficiency of up to 70% not only subverts the traditional view that low-coherence light cannot undergo efficient frequency conversion, but also eliminates one of the primary obstacles to the future development of low-coherence drivers.

VI. TEMPORAL AND SPATIAL BEAM SMOOTHING OF LOW-COHERENCE PULSES

The beam smoothing feature is the ultimate characteristic of a low-coherence beam. With previous low-coherence drivers, limited by various factors such as the acceptance bandwidth of harmonic conversion and the output bandwidth of the amplifier, although the coherence of the output pulses was lower than that of the traditional coherent facilities, it was still high. This imposed sever restrictions on the selection of beam smoothing techniques, and the smoothing effect that was achieved could not fully exploit the advantages of low-coherence light.

The low-coherence laser in our facility has a short time coherence of 300 fs under the conditions of SHG with hundreds of joules. Meanwhile, the far-field characteristics of the low-coherence light are close to those of coherent light, which indicates that the laser

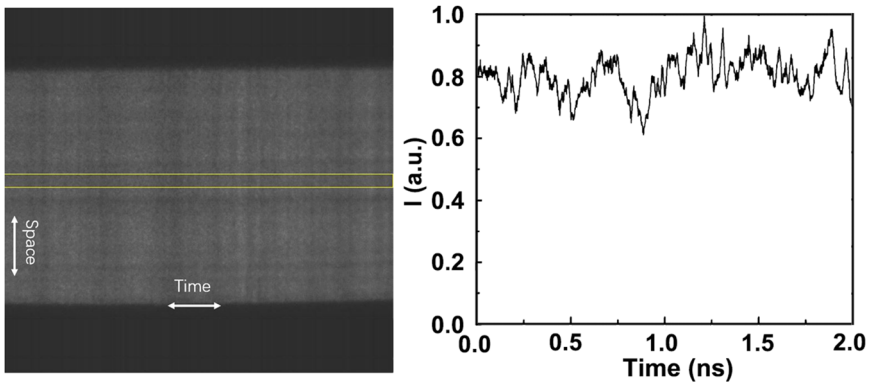

FIG. 21. Temporal intensity distribution of second-harmonic conversion measured by a streak camera with a resolution of 11 ps.

has good spatial coherence. For such light, the use of continuous phase plates (CPPs) or lens arrays (Las) can achieve almost the same results as a design that spatially shapes the two-dimensional intensity distribution. For temporal smoothing, the method of induced spatial incoherence (ISI) is most suitable for such laser facilities. Other possible methods are angular dispersion and polarization smoothing (PS). The speed of smoothing of a low-coherence laser is positively related to its coherence time. Ideally, the rms of a focal spot with integration time T can be calculated as follows:[47]

$$\sigma^2(T) = \frac{\sigma_0^2}{T}, \tag{8}$$

where σ_0^2 is the variance of the focal spot intensity distribution integrated over one coherence time. It is less than 1, typically 0.45 in simulations, which is a consequence of the Gaussian shape of the temporal coherence function. According to Eq. (8), a low-coherence laser with 300-fs coherence time is expected to reach 4% rms in 100 ps. When this approach is used in combination with PS, the rms will be further reduced to 3%.

Currently, our low-coherence laser facility has a variety of beam smoothing capabilities, including CPP, ISI, ISI + LA and ISI + CPP, the last two of which can give a focal spot with good uniformity and high stability.

A. ISI + LA

The combination of ISI and LA[48] is easy to implement on a low-coherence laser. LA and ISI smoothing can be simultaneously achieved by adhering small lenses of different thicknesses, as illustrated in Fig. 22. The focal spot obtained using a coherent laser with ISI + LA is generally the same as that obtained with a LA alone, and is the product of the quasi-near-field distribution of one individual beamlet with the two-dimensional Dirichlet kernel. When a low-coherence laser with coherence time shorter than the time delay induced by the ISI plate is used, the focal spot with ISI + LA will be the intensity superposition of the focal spots of small beamlets. The effect of diffraction of individual beamlets is a major obstacle preventing the ISI + LA method from achieving a focal-spot rms of 1% or lower.

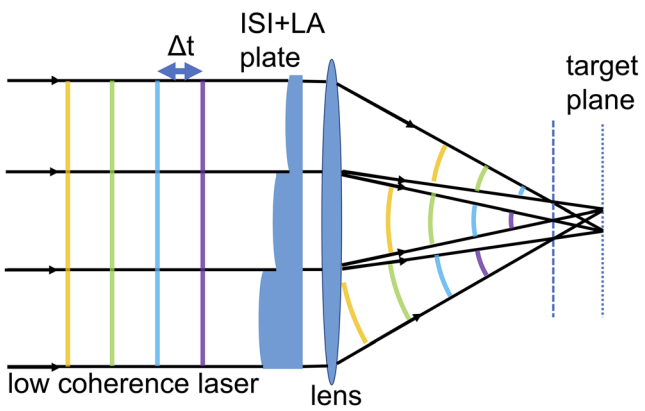

FIG. 22. Schematic of ISI + LA method.

The ISI echelon array should be in one-to-one correspondence with the elements of the LA. ISI causes rapid variation of the instantaneous focal spot and smooths speckles, while the LA controls the overall envelope of the focal spot. A focal spot obtained using ISI + LA is smoothed in all directions with high speed. As an example, focal spots obtained using ISI + LA with 7 × 7 division and different smoothing times are calculated and shown in Fig. 23. To reduce the effect of diffraction in the focal spot, a soft-edged aperture array is used on the LA. The focal spot of ISI + LA with coherent light is similar to the instantaneous focal spot of low-coherence light, as shown in Fig. 23(a). As time increases, the high-frequency components of the nonuniformity of the focal spot are smoothed. An rms of 2% is expected to be achieved after sufficient smoothing time. The simulation also shows that the ISI + LA method is not sensitive to near-field nonuniformity.

The results in Fig. 23 were calculated assuming that the depth of the ISI step was greater than the coherence time. The coherence time is related to the spectral width. When adjusting the spectral width, the ISI step depth is smaller than the coherence time (partial ISI). In this case, the focal spot of partial ISI + LA can be calculated by statistical optics as follows:[49]

$$J(\mathbf{r}_1, \mathbf{r}_2) = \frac{1}{\lambda^2 R^2}\iint J(\mathbf{u}_1, \mathbf{u}_2)\exp\left[-i\frac{k_0}{R}(\mathbf{u}_1\cdot\mathbf{r}_1 - \mathbf{u}_2\cdot\mathbf{r}_2)\right]d\mathbf{u}_1 d\mathbf{u}_2, \tag{9}$$

where $J(\mathbf{r}_1, \mathbf{r}_2)$ is the autocorrelation of the electric field on the focal plane, $J(\mathbf{u}_1, \mathbf{u}_2)$ is the autocorrelation of the near field, and k_0 is the central wavenumber of the incident beam. The intensity distribution on the focal plane can be obtained by choosing $\mathbf{r}_1 = \mathbf{r}_2$ in $J(\mathbf{r}_1, \mathbf{r}_2)$. For ISI + LA, ignoring the interference between beamlets with two or more step delays, the following equation for the focal spot intensity distribution can be derived from Eq. (9):

$$I(\mathbf{r}) = \sum_{jk} I_{jk}(\mathbf{r}) + \gamma\sum_{\Lambda}\exp(i\psi_{jklm})E_{jk}(\mathbf{r})E^*_{mn}(\mathbf{r}), \tag{10}$$

where j, k and m, n index the beamlets, γ is the residual degree of coherence determined from the ISI step depth, $E_{jk}(\mathbf{r})$ is the far field of beamlets j and k, and Λ represents the conditions under which beamlets j and k and beamlets m and n are partially coherent with each other. Owing to the symmetry of the subscripts, $I(\mathbf{r})$ is always real. From Eq. (10), when γ is nonzero, fringes will be caused by interference in the focal spot. An experimental result with partial ISI + LA is shown in Fig. 24(a). The time delay introduced by the ISI + LA plate is about 170 fs, and the coherence time of the beam is 300 fs. γ can be calculated to be 0.29 from the spectrum. As a consequence, there is residual interference in the focal spot, as can be seen in Fig. 24(a). The theoretical result calculated from Eq. (10) is shown in Fig. 24(b) for comparison. The modulation depth is ~0.3, which is close to the coherence degree of 170 fs. The theoretical calculation does not consider wave-front distortion, which can lead to discrepancies in details between the theoretical and experimental results. To eliminate residual interference, the ISI step depth should be larger than the coherence time in beam smoothing of ISI.

Currently, in our laboratory, a 5 × 7 ISI + LA plate and a 6 × 6 ISI + LA plate are used to obtain flat focal spots with sizes of 500 × 700 μm^2 and 300 × 300 μm^2, respectively.

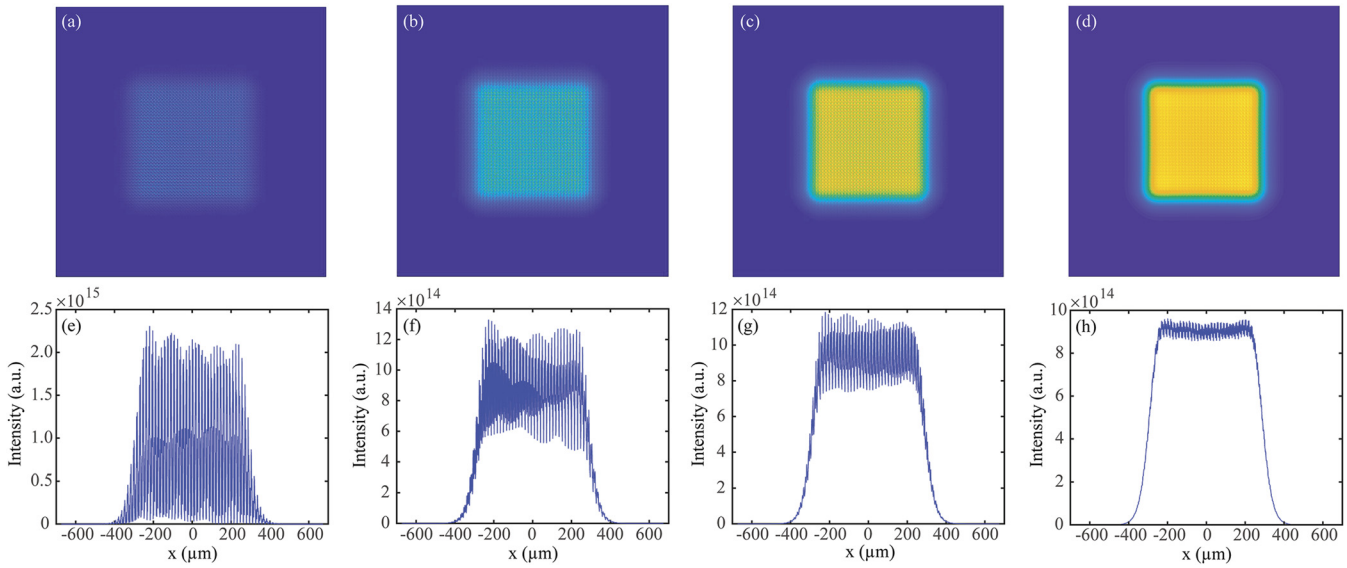

FIG. 23. Focal spots obtained using ISI + LA with smoothing times (a) $T = \tau$, (b) $T = 10\tau$, (c) $T = 100\tau$, and (d) $T = 1000\tau$. (e)–(h) show the corresponding *x*-axis intensity distributions. Reprinted with permission from Zhao *et al.*, Appl. Opt. **58**(8), 2121–2126 (2019). Copyright 2019 Optical Society of America.

B. ISI + CPP

Although ISI + LA can obtain a focal spot with excellent uniformity, there are still some disadvantages to this beam smoothing method. An LA cannot give an arbitrary design of intensity distribution, which is inconvenient when it is necessary to control the uniformity of irradiation in ICF experiments. In addition, the instantaneous focal spot pattern with the ISI + LA method has a spatial period equal to the diffraction limit of the subblock. This periodic modulation may have an adverse effect on the control of instability in beam–target coupling. The ISI + CPP scheme can avoid these drawbacks. The CPP is able to control the focal spot intensity distribution, and the instantaneous focal spot of the ISI + CPP method is more random.

The focal spot distribution with ISI + CPP can be calculated by Fourier optics and statistical optics. A modified Gerchberg–Saxton method is used to design the topography of the CPP with control of the focal-spot PSD. This method avoids the phase unwrapping required in conventional CPP designs by calculating the phase variation in an iterative manner. By applying an appropriate frequency filter to the phase variation between two iterations, the PSD of the focal spot can be controlled, as can the distribution of the CPP. High spatial frequency nonuniformity in the focal spot of the CPP will be eliminated after ISI has been applied. The nonuniformity of the focal spot will be decreased with greater ISI division. However, nonuniformity at low spatial frequencies will be retained in the focal spot if the CPP is of a conventional design. A modified phase plate with discontinuity can be used to obtain a focal spot with better low-spatial-frequency uniformity, but the current design of such plates is difficult to manufacture. Thus, at the present stage, conventional CPPs are still used with ISI for beam smoothing in practical applications. An

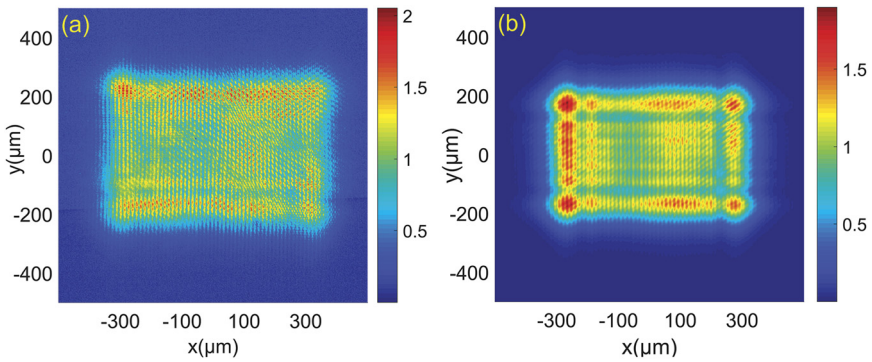

FIG. 24. (a) Experimental focal spot using partial ISI + LA with broadband light. (b) Theoretical result. Reprinted with permission from Li *et al.*, Appl. Opt. **59**(10), 2976–2982 (2020). Copyright 2020 Optical Society of America.

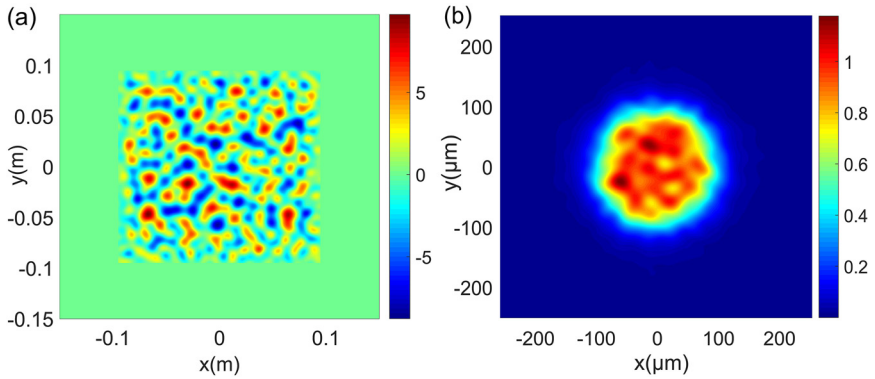

FIG. 25. (a) Phase distribution of a CPP for a 200 μm circular spot. (b) Corresponding simulated focal spot using the CPP with 10 × 10 ISI.

ordinary CPP designed with an eighth-order super-Gaussian far-field profile is shown in Fig. 25(a). A simulation of a focal spot obtained after 10 × 10 ISI division is shown in Fig. 25(b), with a total rms of 0.08 in the central region. Such nonuniformity comes mainly from the slow variation of the intensity profile.

Currently, we have manufactured CPP and ISI plates with different division numbers to obtain a focal spot with a diameter of 200 μm. Additional results on ISI + CPP will be reported in the future publications.

The use of other smoothing methods such as angular spectral dispersion and polarization smoothing on the low-coherence laser is also under consideration, and the components for implementing these methods might be installed in the future.

Using the smoothing methods described above, preliminary experiments on LPI and equation-of-state determinations have been conducted. The results reveal completely different physical effects from those obtained with coherent light.

VII. CONCLUSIONS

In this paper, we have comprehensively reviewed low-coherence laser driver technologies, including low-coherence source generation and control, amplification and propagation of low-coherence pulses, harmonic conversion, and beam smoothing. The most serious technical bottlenecks encountered in such facilities are associated with the need for suitable low-coherence sources, safe and efficient amplification of low-coherence pulses, and efficient harmonic conversion. We have reported several major developments in this area at our institute. We have proposed and experimentally demonstrated a scheme for a low-coherence light facility, which is seeded by a low-coherence front end and amplified by Nd:glass rods and slabs, delivering kilojoule nanosecond-level pulses with a good uniformity and focusing characteristics. Utilizing spectral filtering and control techniques, we can obtain output pulses with a spectral bandwidth of up to 13 nm from a fundamental-wave pulse with kilojoule energy, and the waveform and spectral shape can be adjusted independently. SHG with a bandwidth of 2.9 THz and 70% efficiency has been demonstrated, and the physical mechanism for the frequency conversion of low-coherence pulses has been proposed and confirmed experimentally. To provide a uniform target spot for physical experiments, a beam smoothing scheme for low-coherence pulses has been demonstrated, which shows good uniformity and fast smoothing time. So far, this facility has been operated safely and stably several hundreds of times.

Further improvements will focus mainly on the following aspects:

1. Amplification and propagation characteristics of such low-coherence pulses under the conditions of deep saturation (10 J/cm^2–15 J/cm^2) and high power density (3 GW/cm^2–4 GW/cm^2) will be studied and verified. The laser system will then be scaled up to ~10 kJ.
2. The theory of harmonic conversion of instantaneous broadband low-coherence pulses described above will be improved, with the aim of developing a frequency-doubling technique with larger output bandwidth and higher conversion efficiency that will allow applications using larger apertures.
3. A theory of third-harmonic generation of low-coherence pulses will be developed, and efficient third-harmonic generation techniques for broadband low-coherence pulses will be explored, again with the aim of application to large-aperture projects.
4. Based on the characteristics of low-coherence pulses, beam-smoothing techniques will be developed that match the requirements of large aperture and high fluence.
5. Improvements will be made to beam measurement and characterization capabilities and to control capabilities of low-coherence pulses. A physical experimental research platform based on the low-coherence driver facility will be established for (i) LPI research with low-coherence light; (ii) exploration of ignition driven by SHG; (iii) research on new mechanisms and phenomena involved in the interaction between low-coherence light and matter.[116,117]

We believe that the rapid development of theories and techniques related to low-coherence laser drivers will promote understanding of laser physics and fusion physics, as well as improving laser technology. At the same time, many new and important directions of research will be opened up.

ACKNOWLEDGMENTS

The authors would like to express their heartfelt thanks to many researchers with whom we have had beneficial discussions and who

have made inspired suggestions, including, among others, Academician Weiyan Zhang, Xiaoming Zhang, and Guixue Huang of the China Academy of Engineering Physics; Wanguo Zheng, Yaping Dai, Xiaofeng Wei, and Dong Yang of the Laser Fusion Research Center of the China Academy of Engineering Physics; Yongkun Ding, Shaoping Zhu, Ke Lan, Shiyang Zhou, Hongbo Cai, and Liang Hao of the Institute of Applied Physics and Computational Mathematics; Baoqiang Zhu and Xingqiang Lu of the Shanghai Institute of Optics and Fine Mechanics; Wei Zou of the Institute of Automation; and Rui Wang, Yubao Wang, Fang Lv, and Kai Wu of the 23rd Research Institute of the China Electronics Technology Group Corporation.

REFERENCES

[1]J. W. Goodman, *Speckle Phenomena in Optics: Theory and Applications* (Greenwood Village: Roberts and Company, 2007).

[2]J. D. Rigden and E. I. Gordon, "The granularity of scattered optical maser light," Proc. IRE **50**, 2367-2368 (1962).

[3]W. Burns, C.-L. Chen, and R. Moeller, "Fiber-optic gyroscopes with broad-band sources," J. Lightwave Technol. **1**, 98–105 (1983).

[4]J. Lindl, O. Landen, J. Edwards *et al.*, "Review of the National Ignition Campaign 2009-2012," Phys. Plasmas **21**(2), 020501 (2014).

[5]C. Labaune, "Incoherent light on the road to ignition," Nat. Phys. **3**, 680–682 (2007).

[6]J. D. Lindl, P. Amendt, R. L. Berger *et al.*, "The physics basis for ignition using indirect-drive targets on the National Ignition Facility," Phys. Plasmas **11**(2), 339–491 (2004).

[7]R. S. Craxton, K. S. Anderson, T. R. Boehly *et al.*, "Direct-drive inertial confinement fusion: A review," Phys. Plasmas **22**, 110501 (2015).

[8]Z. Fan, M. Chen, Z. Dai *et al.*, "A new ignition scheme using hybrid indirect-direct drive for inertial confinement fusion," arXiv:1303.1252 [physics.plasm-ph] (2013).

[9]V. A. Smalyuk, D. Shvarts, R. Betti *et al.*, "Role of hot-electron preheating in the compression of direct-drive imploding targets with cryogenic D_2 ablators," Phys. Rev. Lett. **100**, 185005 (2008).

[10]M. Karasik, J. L. Weaver, Y. Aglitskiy *et al.*, "Suppression of laser nonuniformity imprinting using a thin high-*Z* coating," Phys. Rev. Lett. **114**, 085001 (2015).

[11]D. S. Montgomery, "Two decades of progress in understanding and control of laser plasma instabilities in indirect drive inertial fusion," Phys. Plasma **23**(5), 055601 (2016).

[12]S. H. Glenzer, D. H. Froula, L. Divol *et al.*, "Experiments and multiscale simulations of laser propagation through ignition-scale plasmas," Nat. Phys. **3**, 716–719 (2007).

[13]J. Lindl, "Development of the indirect-drive approach to inertial confinement fusion and the target physics basis for ignition and gain," Phys. Plasmas **2**(11), 3933–4024 (1995).

[14]O. A. Hurricane, D. A. Callahan, D. T. Casey *et al.*, "Fuel gain exceeding unity in an inertially confined fusion implosion," Nature **506**, 343–348 (2014).

[15]J. A. Marozas, M. Hohenberger, M. J. Rosenberg *et al.*, "First observation of cross-beam energy transfer mitigation for direct-drive inertial confinement fusion implosions using wavelength detuning at the National Ignition Facility," Phys. Rev. Lett. **120**(8), 085001-1–085001-6 (2018).

[16]Y. Lin, G. N. Lawrence, and T. J. Kessler, "Distributed phase plates for super-Gaussian focal-plane irradiance profiles," Opt. Lett. **20**(7), 764–766 (1995).

[17]Y. Kato, K. Mima, N. Miyanaga *et al.*, "Random phasing of high-power lasers for uniform target acceleration and plasma-instability suppression," Phys. Rev. Lett. **53**, 1057–1060 (1984).

[18]Y. Lin, G. N. Lawrence, and T. J. Kessler, "Design of continuous surface-relief phase plates by surface-based simulated annealing to achieve control of focal-plane irradiance," Opt. Lett. **21**(20), 1703–1705 (1996).

[19]X. Deng, X. Liang, Z. Chen *et al.*, "Uniform illumination of large targets using a lens array," Appl. Opt. **25**(3), 377–381 (1986).

[20]S. Skupsky, R. W. Short, T. Kessler *et al.*, "Improved laser-beam uniformity using the angular dispersion of frequency-modulated light," J. Appl. Phys. **66**(8), 3456–3462 (1989).

[21]S. H. Glenzer, R. L. Berger, L. M. Divol *et al.*, "Reduction of stimulated scattering losses from hohlraum plasmas with laser beam smoothing," Phys. Plasmas **8**(5), 1692–1696 (2001).

[22]R. H. Lehmberg, A. J. Schmitt, and S. E. Bodner, "Theory of induced spatial incoherence," J. Appl. Phys. **62**(7), 2680–2701 (1987).

[23]D. Véron, G. Thiell, and C. Gouédard, "Optical smoothing of the high power PHEBUS Nd-glass laser using the multimode optical fiber technique," Opt. Commun. **97**(3–4), 259–271 (1993).

[24]C. Bibeau, D. R. Speck, R. B. Ehrlich *et al.*, "Power, energy, and temporal performance of the Nova laser facility with recent improvements to the amplifier system," Appl. Opt. **31**(27), 5799–5809 (1992).

[25]V. N. Goncharov, S. P. Regan, E. M. Campbell *et al.*, "National direct-drive program on OMEGA and the National Ignition Facility," Plasma. Phys. Controlled Fusion **59**, 014008 (2017).

[26]M. L. Spaeth, K. R. Manes, M. Bowers *et al.*, "National Ignition Facility laser system performance," Fusion Sci. Technol. **69** (1), 366–394 (2016).

[27]N. Fleurot, C. Cavailler, and J. L. Bourgade, "The Laser Mégajoule (LMJ) project dedicated to inertial confinement fusion: Development and construction status," Fusion Eng. Des. **74**(1-4), 147–154 (2005).

[28]C. Yamanaka, "Gekko XII glass laser system," Rev. Laser Eng. **11**(8), 586–611 (1983).

[29]S. Jiang, F. Wang, Y. Ding *et al.*, "Experimental progress of inertial confinement fusion based at the ShenGuang-III laser facility in China," Nucl. Fusion **59**, 032006 (2019).

[30]J. E. Rothenberg, "Polarization beam smoothing for inertial confinement fusion," J. Appl. Phys. **87**(8), 3654 (2000).

[31]A. N. Mostovych, S. P. Obenschain, J. H. Gardner *et al.*, "Brillouin scattering measurements from plasmas irradiated with spatially and temporally incoherent laser light," Phys. Rev. Lett. **59**(11), 1193–1196 (1987).

[32]J. D. Moody, P. Michel, L. Divol *et al.*, "Multistep redirection by cross-beam power transfer of ultrahigh-power lasers in a plasma," Nat. Phys. **8**, 344–349 (2012).

[33]R. Betti and O. A. Hurricane, "Inertial-confinement fusion with lasers," Nat. Phys. **12**, 435–448 (2016).

[34]M. S. Pronko, R. H. Lehmberg, S. Obenschain *et al.*, "Efficient second harmonic conversion of broad-band high-peak-power Nd:glass laser radiation using large-aperture KDP crystal in quadrature," IEEE J. Quantum Electron. **26**(2), 337–347 (1990).

[35]M. Nakatsuka, N. Miyanaga, T. Kanabe *et al.*, "Partially coherent light sources for ICF experiment," Proc. SPIE **1870**, 151–162 (1993).

[36]S. I. Fedotov, L. P. Feoktistov, M. V. Osipov *et al.*, "Lasers for ICF with a controllable function of mutual coherence of radiation," J. Russ. Laser Res. **25**(1), 79–92 (2004).

[37]E. L. Dewald, S. H. Glenzer, O. L. Landen *et al.*, "First laser–plasma interaction and hohlraum experiments on the National Ignition Facility," Plasma Phys. Controlled Fusion **47**, B405–B417 (2005).

[38]R. Zhang, H. Jia, X. Tian *et al.*, "Research of beam conditioning technologies using continuous phase plate, multi-FM smoothing by spectral dispersion and polarization smoothing," Opt. Laser. Eng. **85**, 38–47 (2016).

[39]A. N. Starodub, S. I. Fedotov, A. A. Kozhevnikova, *et al.*, "Interaction of partially coherent laser radiation with matter," Proc. SPIE **6595**, 65950A (2007).

[40]C. Dorrer, E. M. Hill, and J. D. Zuegel, "High-energy parametric amplification of spectrally incoherent broadband pulses," Opt. Express **28**(1), 451–471 (2020).

[41]J. W. Bates, J. F. Myatt, J. G. Shaw *et al.*, "Mitigation of cross-beam energy transfer in inertial-confinement-fusion plasmas with enhanced laser bandwidth," Phys. Rev. E **97**, 061202 (2018).

[42]Y. Zhao, S. Weng, M. Chen *et al.*, "Stimulated Raman scattering excited by incoherent light in plasma," Matter Radiat. Extremes **2**, 190–196 (2017).

[43]D. Rao, Y. Gao, Y. Cui *et al.*, "1 μJ nanosecond low-coherent laser source with precise temporal shaping and spectral control," Opt. Laser Technol. **122**, 105850 (2020).

[44]Y. Cui, Y. Gao, D. Rao *et al.*, "High-energy low-temporal-coherence instantaneous broadband pulse system," Opt. Lett. **44**(11), 2859–2862 (2019).
[45]L. Ji, X. Zhao, D. Liu *et al.*, "High-efficiency second-harmonic generation of low-temporal-coherent light pulse," Opt. Lett. **44**(17), 4359–4362 (2019).
[46]X. H. Zhao, L. L. Ji, D. Liu *et al.*, "Second-harmonic generation of temporally low-coherence light," APL Photonics **5**(9), 091301 (2020).
[47]F. J. Li, Y. Q. Gao, X. H. Zhao *et al.*, "Induced spatial incoherence combined with continuous phase plate for the improved beam smoothing effect," Opt. Eng. **57**, 066117 (2018).
[48]X. Zhao, Y. Gao, F. Li *et al.*, "Beam smoothing by a diffraction-weakened lens array combining with induced spatial incoherence," Appl. Opt. **58**(8), 2121–2126 (2019).
[49]F. Li, Y. Gao, X. Zhao *et al.*, "Experiment and theory of beam smoothing using induced spatial incoherence with lens array," Appl. Opt. **59**(10), 2976–2982 (2020).
[50]Y. Gao, L. Ji, X. Zhao *et al.*, "Low-coherence high-power laser facility" (submitted).
[51]P. J. Wisoff, M. W. Bowers, G. V. Erbert *et al.*, "NIF injection laser system," Proc. SPIE **5341**, 146–155 (2004).
[52]M. Bowers, S. Burkhart, S. Cohen *et al.*, "The injection laser system on the National Ignition Facility," Proc. SPIE **6451**, 64511M (2007).
[53]W. Fan, Y. Jiang, J. Wang *et al.*, "Progress of the injection laser system of SG-II," High Power Laser Sci. **6**, e34 (2018).
[54]H. Nakano, T. Kanabe, K. Yagi *et al.*, "Amplification and propagation of partially coherent amplified spontaneous emission from Nd:glass," Opt. Commun. **78**(2), 123 (1990).
[55]H. Nakano, K. Tsubakimoto, N. Miyanaga *et al.*, "Spectrally dispersed amplified spontaneous emission for improving irradiation uniformity into high power Nd: glass laser system," J. Appl. Phys. **73**(5), 2122 (1993).
[56]H. Nakano, N. Miyanaga, K. Yagi *et al.*, "Partially coherent light generated by using single and multimode optical fibers in a high-power Nd:glass laser system," Appl. Phys. Lett. **63**(5), 580 (1993).
[57]V. G. Dmitriev, M. V. Osipov, V. N. Puzyrev *et al.*, "Nonlinear optical conversion of Nd:glass laser multimode radiation into the second harmonic in KDP crystal," J. Phys. B: At., Mol. Opt. Phys. **45**(16), 165401 (2012).
[58]N. A. Fleurot, M. A. Andre, P. Estraillier *et al.*, "Output pulse and energy capabilities of the PHEBUS laser facility," paper presented at the Industrial and Scientific Uses of High-Power Lasers, 1991.
[59]L. Videau, A. C. L. Boscheron, J. C. Garnier *et al.*, "Recent results of optical smoothing on the PHEBUS laser," Proc. SPIE **3047**, 757 (1997).
[60]C. A. Haynam, P. J. Wegner, J. M. Auerbach *et al.*, "National Ignition Facility laser performance status," Appl. Opt. **46**(16), 3276 (2007).
[61]L. M. Frantz and J. S. Nodvik, "Theory of pulse propagation in a laser amplifier," J. Appl. Phys. **34**, 2346 (1963).
[62]D. Veron, G. Thiell, C. Gouedard *et al.*, "Focal spot smoothing by amplification of reduced coherence pulse in the high power Nd-glass PHEBUS laser," Proc. SPIE **1870**, 140–150 (1993).
[63]P. Donnat, C. Gouédard, D. Veron *et al.*, "Induced spatial incoherence and nonlinear effects in Nd:glass amplifiers," Opt. Lett. **17**(5), 331–333 (1992).
[64]L. Videau, E. Bar, C. Rouyer *et al.*, "Control of the amplification of large band amplitude modulated pulses in Nd-glass amplifier chain," Proc. SPIE **3492**, 277–284 (1998).
[65]J. Garnier, J. P. Fouque, L. Videau *et al.*, "Amplification of broadband incoherent light in homogeneously broadened media in the presence of Kerr nonlinearity," J. Opt. Soc. Am. B **14**(10), 2563–2569 (1997).
[66]J. Garnier, L. Videau, C. Gouédard *et al.*, "Propagation and amplification of incoherent pulses in dispersive and nonlinear media," J. Opt. Soc. Am. B **15**(11), 2773–2781 (1998).
[67]P. A. Franken, A. E. Hill, C. W. Peters *et al.*, "Generation of optical harmonics," Phys. Rev. Lett. **7**(4), 118–119 (1961).
[68]N. Bloembergen and P. S. Pershan, "Light waves at boundary of nonlinear media," Phys. Rev. **128**(2), 606–622 (1962).
[69]R. Eckardt and J. Reintjes, "Phase matching limitations of high efficiency second harmonic generation," IEEE J. Quantum Electron. **20**(10), 1178–1187 (1984).
[70]O. E. Martinez, "Achromatic phase matching for second harmonic generation of femtosecond pulses," IEEE J. Quantum Electron. **25**, 2464–2468 (1989).
[71]G. Szabo and Z. Bor, "Broadband frequency doubler for femtosecond pulses," Appl. Phys. B **50**, 51–54 (1990).
[72]B. A. Richman, S. E. Bisson, R. Trebino *et al.*, "Efficient broadband second-harmonic generation by dispersive achromatic nonlinear conversion using only prisms," Opt. Lett. **23**, 497–499 (1998).
[73]M. Brown, "Increased spectral bandwidths in nonlinear conversion processes by use of multicrystal designs," Opt. Lett. **23**, 1591–1593 (1998).
[74]S. Ashihara, T. Shimura, and K. Kuroda, "Group-velocity matched second-harmonic generation in tilted quasiphase-matched gratings," J. Opt. Soc. Am. B **20**, 853–856 (2003).
[75]G. Y. Wang and E. M. Garmire, "High-efficiency generation of ultrashort second-harmonic pulses based on the Cerenkov geometry," Opt. Lett. **19**, 254–256 (1994).
[76]L. E. Nelson, S. B. Fleischer, G. Lenz *et al.*, "Efficient frequency doubling of a femtosecond fiber laser," Opt. Lett. **21**, 1759–1761 (1996).
[77]X. Liu, L. Qian, and F. W. Wise, "Efficient generation of 50-fs red pulses by frequency doubling in LiB_3O_5," Opt. Commun. **144**, 265–268 (1997).
[78]N. E. Yu, J. H. Ro, M. Cha *et al.*, "Broadband quasi-phase-matched second-harmonic generation in MgO-doped periodically poled $LiNbO_3$ at the communications band," Opt. Lett. **27**, 1046–1048 (2002).
[79]M. S. Webb, D. Eimerl, and S. P. Velsko, "Wavelength insensitive phase-matched second-harmonic generation in partially deuterated KDP," J. Opt. Soc. Am. B **9**, 1118–1127 (1992).
[80]L. Ji, B. Zhu, C. Liu *et al.*, "Optimization of quadrature frequency conversion with type-II KDP for second harmonic generation of the nanosecond chirp pulse at 1053 nm," Chin. Opt. Lett. **12**(3), 031902 (2014).
[81]D. Eimerl, J. M. Auerbach, C. E. Barker *et al.*, "Multicrystal designs for efficient third-harmonic generation," Opt. Lett. **22**(16), 1208–1210 (1997).
[82]"Optomechanical system," in *OMEGA System Operations Manual: Volume I–System Description* (Laboratory for Laser Energetics, University of Rochester, 2003), Chap. 5.
[83]A. Babushkin, R. S. Craxton, S. Oskoui *et al.*, "Demonstration of the dual-tripler scheme for increased-bandwidth third-harmonic generation," Opt. Lett. **23**, 927–929 (1998).
[84]F. Raoult, A. C. L. Boscheron, D. Husson *et al.*, "Ultrashort, intense ultraviolet pulse generation by efficient frequency tripling and adapted phase matching," Opt. Lett. **24**(5), 354–356 (1999).
[85]A. C. L. Boscheron, C. J. Sauteret, and A. Migus, "Efficient broadband sum frequency based on controlled phase-modulated input fields: Theory for 351-nm ultrabroadband or ultrashort-pulse generation," J. Opt. Soc. Am. B **13**, 818–826 (1996).
[86]L. J. Qian, "Chirp matched third-harmonic generation for broad-band laser," Acta. Opt. Sin. **15**(6), 662–664 (1995).
[87]Y. Chen, P. Yuan, and L. Qian, "A broadband frequency-tripling scheme for an Nd:glass laser-based chirped-pulse amplification system: An approach for efficiently generating ultraviolet petawatt pulses," J. Opt. **13**(7), 075205 (2011).
[88]H. Zhu, T. Wang, W. Zheng *et al.*, "Efficient second harmonic generation of femtosecond laser at 1 μm," Opt. Express **12**(10), 2150–21555 (2004).
[89]E. Rozenberg and A. Arie, "Broadband and robust adiabatic second-harmonic generation by a temperature gradient in birefringently phase-matched lithium triborate crystal," Opt. Lett. **44**(13), 3358–3361 (2019).
[90]P. Yuan, L. Qian, W. Zheng *et al.*, "Broadband frequency tripling based on segmented partially deuterated KDP crystals," J. Opt. A: Pure Appl. Opt. **9**(11), 1082–1086 (2007).
[91]S. Skupsky and K. Lee, "Uniformity of energy deposition for laser driven fusion," J. Appl. Phys. **54**, 3662–3671 (1983).
[92]S. N. Dixit, I. M. Thomas, B. W. Woods *et al.*, "Random phase plates for beam smoothing on the Nova laser," Appl. Opt. **32**(14), 2543–2554 (1993).
[93]J. K. Terrance, L. Ying, J. J. Armstrong *et al.*, "Phase conversion of lasers with low-loss distributed phase plates," Proc. SPIE **1870**, 95 (1993).
[94]S. N. Dixit, J. K. Lawson, K. R. Manes *et al.*, "Kinoform phase plates for focal plane irradiance profile control," Opt. Lett. **19**(6), 417–419 (1994).

[95]J. A. Marozas, "Fourier transform-based continuous phase-plate design technique: A high-pass phase-plate design as an application for OMEGA and the National Ignition Facility," J. Opt. Soc. Am. A **24**(1), 74–83 (2007).
[96]R. H. Lehmberg and S. P. Obenschain, "Use of induced spatial incoherence for uniform illumination of laser fusion targets," Opt. Commun. **46**, 27–31 (1983).
[97]T. A. Peyser, C. K. Manka, S. P. Obenschain *et al.*, "Reduction of $3\omega_0/2$ emission from laser-produced plasmas with broad bandwidth, induced spatial incoherence at 0.53 μm," Phys. Fluids B **3**(6), 1479–1484 (1991).
[98]S. Skupsky and R. S. Craxton, "Irradiation uniformity for high-compression laser-fusion experiments," Phys. Plasmas **6**(5), 2157–2163 (1999).
[99]S. P. Regan, J. A. Marozas, R. S. Craxton *et al.*, "Performance of 1-THz-bandwidth two-dimensional smoothing by spectral dispersion and polarization smoothing of high-power, solid-state laser beams," J. Opt. Soc. Am. B **22**(5), 998 (2005).
[100]G. Miyaji, N. Miyanaga, S. Urushihara *et al.*, "Three-directional spectral dispersion for smoothing of a laser irradiance profile," Opt. Lett. **27**(9), 725–727 (2002).
[101]J. E. Rothenberg, "Comparison of beam-smoothing methods for direct-drive inertial confinement fusion," J. Opt. Soc. Am. B **14**(7), 1664–1671 (1997).
[102]D. M. Pennington, S. N. Dixit, T. L. Weiland *et al.*, "Implementation and performance of beam smoothing on 10 beams of the Nova laser," Proc. SPIE **3047**, 725–735 (1997).
[103]T. E. Gunderman, J. Lee, T. J. Kessler *et al.*, "Liquid crystal distributed polarization rotator for improved uniformity of focused laser light," in Conference on Lasers and Electro-Optics, OSA Technical Digest. **7**, CTHC7 (1990).
[104]K. Tsubakimoto, M. Nakatsuka, H. Nakano *et al.*, "Suppression of interference speckles produced by a random phase plate, using a polarization control plate," Opt. Commun. **91**, 9–12 (1992).
[105]T. R. Boehly, V. A. Smalyuk, D. D. Meyerhofer *et al.*, "Reduction of laser imprinting using polarization smoothing on a solid-state fusion laser," J. Appl. Phys. **85**(7), 3444 (1999).
[106]S. P. Obenschain, S. E. Bodner, D. Colombant *et al.*, "The Nike KrF laser facility: Performance and initial target experiments," Phys. Plasmas **3**, 2098–2107 (1996).
[107]D. Véron, H. Ayral, C. Gouedard *et al.*, "Optical spatial smoothing of Nd-glass laser beam," Opt. Commun. **65**, 42–46 (1988).
[108]J. Faure, J.-R. Marquès, V. Malka *et al.*, "Dynamics of Raman instabilities using chirped laser pulses," Phys. Rev. E **63**, 065401 (2001).
[109]B. J. Albright, L. Yin, and B. Afeyan, "Control of stimulated Raman scattering in the strongly nonlinear and kinetic regime using spike trains of uneven duration and delay," Phys. Rev. Lett. **113**, 045002 (2014).
[110]J. Park and X. Li, "Theoretical and numerical analysis of superluminescent diodes," J. Lightwave Technol. **24**(6), 2473 (2006).
[111]G. A. Alphonse, D. B. Gilbert, M. G. Harvey *et al.*, "High-power superluminescent diodes," IEEE J. Quantum Electron. **24**(12), 2454–2457 (1988).
[112]T. Takayama, O. Imafuji, Y. Kouchi *et al.*, "100-mW high-power angled-stripe superluminescent diodes with a new real refractive-index-guided self-aligned structure," IEEE J. Quantum Electron. **32**(11), 1981–1987 (1996).
[113]L. Wang and A. M. Weiner, "Programmable spectral phase coding of an amplified spontaneous emission light source," Opt. Commun. **167**(1-6), 211–224 (1999).
[114]V. Torres-Company, J. Lancis, and P. Andres, "Arbitrary waveform generator based on all-incoherent pulse shaping," IEEE Photonics Technol. Lett. **18**(24), 2626–2628 (2006).
[115]C. Dorrer, "Statistical analysis of incoherent pulse shaping," Opt. Express **17**(5), 3341–3352 (2009).
[116]K. Lan and P. Song, "Foam Au driven by $4\omega - 2\omega$ ignition laser pulse for inertial confinement fusion," Phys. Plasmas **24**, 052707 (2017).
[117]Y.-H. Chen, K. Lan, W. Zheng *et al.*, "High coupling efficiency of foam spherical hohlraum driven by 2ω laser light," Phys. Plasmas **25**, 022702 (2018).